Molecular Therapy
Original Article

Synapsin III gene silencing redeems alpha-synuclein transgenic mice from Parkinson's disease-like phenotype

Gaia Faustini,[1] Francesca Longhena,[1] Anna Masato,[2] Valentina Bassareo,[3] Roberto Frau,[3] Therése Klingstedt,[4] Hamid Shirani,[4] Viviana Brembati,[1] Edoardo Parrella,[1] Marika Vezzoli,[1] K. Peter R. Nilsson,[4] Marina Pizzi,[1] Maria Grazia Spillantini,[5] Luigi Bubacco,[2] and Arianna Bellucci[1]

[1]Department of Molecular and Translational Medicine, University of Brescia, Viale Europa 11, 25123 Brescia, Italy; [2]Department of Biology, University of Padova, Via Ugo Bassi 58b, 35121 Padua, Italy; [3]Department of Biomedical Sciences, University of Cagliari, Cittadella Universitaria Blocco A, Cagliari, 09124 Cagliari, Italy; [4]Department of Physics, Chemistry and Biology, Linköping University, 581 83 Linköping, Sweden; [5]Department of Clinical Neurosciences, University of Cambridge, Clifford Albutt Building, Cambridge CB2 0AH, UK

Fibrillary aggregated α-synuclein (α-syn) deposition in Lewy bodies (LB) characterizes Parkinson's disease (PD) and is believed to trigger dopaminergic synaptic failure and a retrograde terminal-to-cell body neuronal degeneration. We described that the neuronal phosphoprotein synapsin III (Syn III) cooperates with α-syn to regulate dopamine (DA) release and can be found in the insoluble α-syn fibrils composing LB. Moreover, we showed that α-syn aggregates deposition, and the associated onset of synaptic deficits and neuronal degeneration occurring following adeno-associated viral vectors-mediated overexpression of human α-syn in the nigrostriatal system are hindered in Syn III knock out mice. This supports that Syn III facilitates α-syn aggregation.
Here, in an interventional experimental design, we found that by inducing the gene silencing of Syn III in human α-syn transgenic mice at PD-like stage with advanced α-syn aggregation and overt striatal synaptic failure, we could lower α-syn aggregates and striatal fibers loss. In parallel, we observed recovery from synaptic vesicles clumping, DA release failure, and motor functions impairment. This supports that Syn III consolidates α-syn aggregates, while its downregulation enables their reduction and redeems the PD-like phenotype. Strategies targeting Syn III could thus constitute a therapeutic option for PD.

INTRODUCTION

The key neuropathological hallmarks of Parkinson's disease (PD) are degeneration of nigrostriatal dopaminergic neurons and presence of Lewy bodies (LB), intraneuronal inclusions mainly composed of fibrillary α-synuclein (α-syn).[1] The deposition of α-syn is considered to play a causative role in the onset of motor and non-motor symptoms of PD, thus suggesting that α-syn aggregation-related synaptic dysfunctions may be the primary cause of neurodegeneration in this disorder.[2,3] In particular, the pivotal role exerted by α-syn within dopaminergic neurons as a regulator of neurotransmitter synthesis, vesicle storage, reuptake, and release[4–6] hints that this cell population can be particularly vulnerable to α-syn aggregation. Indeed, there is compelling evidence that α-syn aggregation can first compromise striatal synaptic functions and then induce a retrograde terminal-to-cell body neuronal degeneration in the *substantia nigra*.[7]

We previously described that synapsin III (Syn III), a synaptic phosphoprotein negatively regulating dopamine (DA) release,[6,8] is present in α-syn filaments purified from postmortem brains of sporadic PD patients, presenting with co-pathology composed of both proteins.[1,9] We also observed fibrillary Syn III/α-syn co-aggregates in the brain of transgenic mice expressing human C-terminally truncated (1–120) α-syn under the guidance of the rat tyrosine hydroxylase (TH) promoter on the C57BL/6JOlaHsd α-syn null background (SYN120 tg).[10] Moreover, we have described that the formation of α-syn aggregates as well as the associated onset of nigrostriatal synaptic injury and neuronal degeneration in an adeno-associated viral vector (AAV)-based mouse model overexpressing human wild type (wt) α-syn, is hampered in the absence of Syn III.[11] This evidence supports that Syn III acts as a promoting factor for α-syn aggregation.

Interestingly, we also observed that the monoamine reuptake inhibitor methylphenidate (MPH), known to counteract gait hypokinesia and freezing in advanced PD,[12,13] specifically restores motor abilities in SYN120 tg mice at pathological stage.[10] Of note, this MPH effect is not related to DA transporter (DAT) inhibition, but relies on the presence of Syn III.[10] Consistently, by generating a fluorescent cell permeable MPH derivative, we were able to detect a direct interaction between MPH and Syn III in cells in culture by fluorescence resonance energy transfer (FRET).[14] In addition, we observed that

Received 26 May 2021; accepted 12 January 2022;
https://doi.org/10.1016/j.ymthe.2022.01.021.

Correspondence: Arianna Bellucci, PhD, Division of Pharmacology, Department of Molecular and Translational Medicine, University of Brescia, Viale Europa No. 11, 25123 Brescia, Italy.
E-mail: arianna.bellucci@unibs.it

Please cite this article in press as: Faustini et al., Synapsin III gene silencing redeems alpha-synuclein transgenic mice from Parkinson's disease-like phenotype, Molecular Therapy (2022), https://doi.org/10.1016/j.ymthe.2022.01.021

MPH promotes the interaction between Syn III and a specific α-helical conformation of α-syn owning low aggregation propensity.[10] This effect is contrary to that of Syn III, which instead appears to promote α-syn aggregation. All together, these findings point to Syn III as a druggable target for PD.

To validate this hypothesis, we established an interventional experimental design aimed at addressing whether Syn III manipulation at a pathological stage in which α-syn aggregates *in vivo* are already formed and relate with the onset of an early PD-like phenotype can exert a disease-modifying effect. In particular, we investigated whether and how Syn III knock down by RNA interfering (RNAi) in the nigrostriatal system of SYN120 tg mice at early PD-like pathological stage could affect α-syn aggregation, the onset of motor deficits, and nigrostriatal terminals dysfunction and degeneration. RNAi was performed by bilateral stereotaxic injection of AAV expressing a short hairpin (shRNA) sequence for mouse Syn III gene (Syn3) (AAV-shSynIII) in the *substantia nigra* of 12-month-old SYN120 tg mice or C57BL/6JOlaHsd and C57BL/6J wt littermates. At this age, the SYN120 tg mice already display marked deposition of insoluble α-syn/Syn III aggregates and advanced synaptic failure, while frank motor deficits become more apparent between 16 and 18 months of age.[6,10,15,16] Age-matched control groups of SYN120 tg, C57BL/6OlaHsd, and C57BL/6J mice were injected with AAV expressing non-silencing control RNA sequences (AAV-shNSC). Animals were analyzed at 4 months after AAV injections to evaluate motor functions (by open field and beam walking test) and striatal DA release in freely moving conditions by vertical microdialysis. Then, they were sacrificed to collect brains to study α-syn aggregation, protection of striatal TH-positive fibers, and synaptic vesicles (SVs) organization at striatal terminals as a readout of a possible disease-modifying effect of Syn III gene silencing.

We found that the SYN120 tg mice injected with AAV-shSynIII exhibited a reduction of α-syn aggregates in the *substantia nigra* and *striatum*. In this latter brain area, fibers were spared from degeneration and terminals from SV clumping. Finally, Syn III gene silencing allowed a marked recovery of basal, depolarization-dependent, and cocaine-stimulated DA release in the *striatum* of SYN120 tg mice, which also displayed increased motility in the open field and beam walking test. These results indicate that Syn III reduction rescued the SYN120 tg mice from α-syn aggregates deposition and the associated synaptic and motor dysfunction. Overall, our findings support that therapeutic strategies targeting Syn III could be beneficial for the treatment of diseases exhibiting α-syn aggregation like PD.

RESULTS

AAV-mediated Syn III RNAi efficiently reduced the expression and levels of Syn III

First, we checked the localization of the enhanced green fluorescent protein (eGFP) reporter of both AAV-shNSC or AAV-shSynIII in the *substantia nigra* and *striatum* of SYN120 tg mice 4 months after stereotaxic injections by immunohistochemistry and bright-field microscopy. We found that eGFP immunopositivity was localized in the *substantia nigra* and *striatum*, thus supporting the correct site for AAV injections (Figure 1A).

In the same animals, we also evaluated whether the eGFP reporter signal co-localized with the TH-immunopositive nigrostriatal neurons of the *substantia nigra* by confocal microscopy. We found that AAV-shNSC- and AAV-shSynIII-associated eGFP reporter signal co-localized with some of the TH-positive neuronal cell bodies and fibers in the *substantia nigra* and the *striatum*, respectively (Figure 1B). This finding supports the correct expression of our shRNA in nigrostriatal neurons. Then, we estimated the efficiency of infection of the nigral TH-positive neurons with either AAV-shNSC or AAV-shSynIII in the C57BL/6JOlaHsd, C57BL/6J, and SYN120 tg mice at 4 weeks following the injections. In particular, to estimate the percent of TH-immunoreactive cells or processes exhibiting eGFP reporter signal, we quantified the average eGFP/TH co-localizing area, normalized versus the total TH-immunopositive area in serial sections from the *substantia nigra* of the AAV-shNSC- or AAV-shSynIII-injected animals. Results from this analysis indicated that in the three mouse lines the percentage of TH-immunoreactive cells or processes exhibiting eGFP reporter signal was about 40% for the animals injected with AAV-shNSC, while it ranged around 30% for those injected with AAV-shSynIII (Figure S1A).

Subsequently, we evaluated the efficiency of Syn III silencing in C57BL/6J, C57BL/6JOlaHsd, and SYN120 tg mice 4 months after the injection of AAV-shNSC or AAV-shSynIII by Syn III and TH double immunofluorescent labeling. A significant decrease of Syn III-immunopositive area was detected in the *substantia nigra* of C57BL/6J, C57BL/6JOlaHsd, and SYN120 tg mice injected with AAV-shSynIII when compared to their respective AAV-shNSC-injected littermates (Figure 1C). By quantifying TH-immunopositive area in the *substantia nigra* of the C57BL/6J, C57BL/6JOlaHsd, and SYN120 tg mice, we found that neither AAV-shNSC nor AAV-shSynIII infection induced TH-positive neuronal loss or shrinkage in the different mouse lines (Figure S1B). In spite of the fact that aged SYN120 tg mice do not display a frank TH-positive neuronal loss in the substantia nigra,[17] this analysis showed a significant reduction of TH-immunopositive area in the AAV-shNSC-injected SYN120 tg mice when compared with C57BL/6J and C57BL/6JOlaHsd animals, which is supportive of the occurrence of neuronal shrinkage. Of note, the analysis also showed that the SYN120 tg mice injected with AAV-shSynIII exhibited an increase of TH-positive area when compared to their littermates who received AAV-shNSC injections (Figure S1B). This supports that Syn III gene silencing exerted a neuroprotective effect on the nigral neurons of the SYN120 tg mice.

The analysis of total Syn III-positive area in the *striatum* confirmed an efficient gene silencing of Syn III also in the nigrostriatal terminals of the three mouse lines injected with AAV-shSynIII when compared with those injected with AAV-shNSC (Figure 2A). Interestingly, we also observed that the average size of Syn III-immunoreactive areas, taken into account as an index of Syn III-positive aggregates formation,[10,11] was significantly reduced only in the *striatum* of

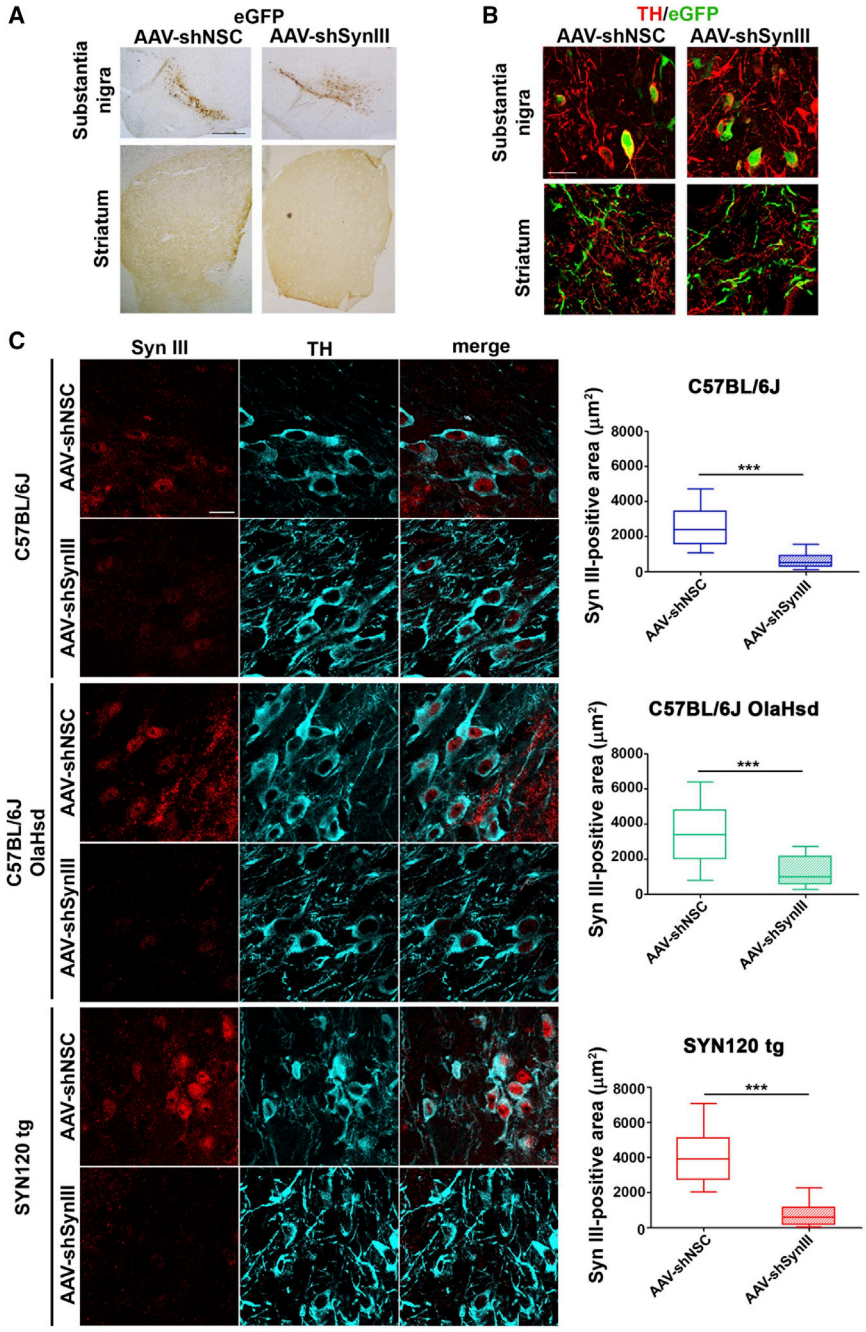

Figure 1. Evaluation of the efficiency and specificity of Syn III silencing in the nigrostriatal system of AAV-shNSC- and AAV-shSynIII-injected mice

(A) Representative images showing eGFP-immunolabeling in the *substantia nigra* and *striatum* of SYN120 tg mice injected with AAV-shNSC or AAV-shSynIII. Scale bar: 100 μm. (B) Representative images show eGFP signal in the TH-immunopositive neurons of the *substantia nigra* and fibers of the *striatum* of AAV-shNSC- and AAV-shSynIII-injected SYN120 tg mice. Scale bar: 20 μm. (C) Syn III-immunopositive signal in the TH-positive neurons of the *substantia nigra* of C57BL/6J, C57BL/6JOlaHsd, and SYN120 tg mice injected with either AAV-shSNC or AAV-shSynIII. Graphs show results from the analysis of the Syn III-positive area in the *substantia nigra* of AAV-shSynIII-injected mice when compared with the AAV-shNSC-injected littermates of the three mouse lines. Data are expressed as positive area in μm^2. Boxplots represent the distribution of the 75%, 50%, and 25% of the values. Whiskers indicate the upper and lower extreme of the dataset. Please note the significant decrease of Syn III in AAV-shSynIII-injected mice (***, –2,221 μm^2, $P < 0.001$ in C57BL/5J mice; ***, –2,081 μm^2, $P < 0.001$ in C57BL/6JOlaHsd mice; ***, –3,057 μm^2, $P < 0.001$ in SYN120 tg mice). Unpaired Welch's t test. $n = 4/5$ for each group. Scale bar: 20 μm.

AAV-shSynIII-injected SYN120 tg mice when compared with AAV-shNSC-injected littermates, but not in that of C57BL/6J or C57BL/6JOlaHsd animals.

The specificity of Syn III silencing was then evaluated by quantitative real-time PCR (qRT-PCR). In particular, we determined the expression of Syn III and also of its orthologues Syn II and Syn I to confirm the selectivity of our shRNA (Figure 2B). We found that AAV-shSynIII injections reduced Syn III expression in the *substantia nigra* of C57BL/6J, C57BL/6JOlaHsd, and SYN120 tg mice when compared with AAV-shNSC-injected littermates. In parallel, we observed that Syn II relative expression was comparable in the AAV-shSynIII and AAV-shNSC-injected C56BL/6J, C57BL/6JOlaHsd, and SYN120 tg mice, thus supporting the specificity of Syn III gene silencing. Interestingly, the analysis of Syn I relative gene expression suggested the occurrence of a compensatory increase of Syn I following Syn III gene silencing only in the AAV-shSynIII-injected SYN120 tg mice when compared with AAV-shNSC-injected animals, while the other mouse lines, despite a tendency to the increase of Syn I, did not show significant changes.

Finally, the levels of Syn III, Syn I, and Syn II in the nigrostriatal system were investigated by western blot (wb) analysis. In line with the immunolabeling and qRT-PCR data, we observed a significant decrease of Syn III levels in the AAV-shSynIII-injected *substantia nigra* (Figure 3A) and *striatum* (Figure 3B) of C57BL/6J, C57BL/6JOlaHsd, and SYN120 tg mice when compared with those of AAV-shNSC-injected controls. Consistently with our previous findings,[10] these wb studies confirmed that the levels of Syn III in the *substantia nigra* and *striatum* of AAV-shNSC-injected C57BL/6JOlaHsd and SYN120 tg control mice were significantly higher than those of C57BL/6J littermates. In parallel,

Please cite this article in press as: Faustini et al., Synapsin III gene silencing redeems alpha-synuclein transgenic mice from Parkinson's disease-like phenotype, Molecular Therapy (2022), https://doi.org/10.1016/j.ymthe.2022.01.021

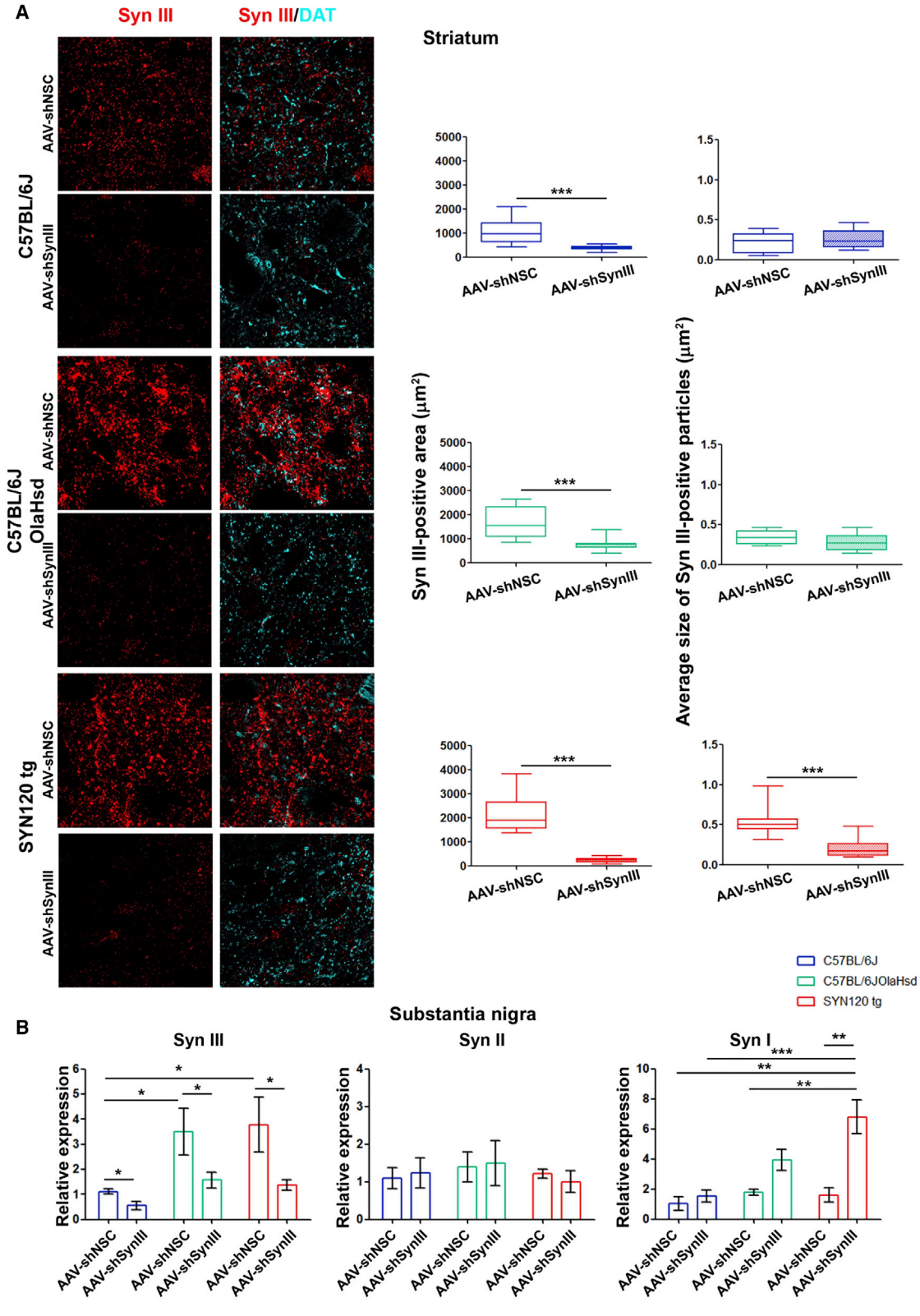

(legend on next page)

Please cite this article in press as: Faustini et al., Synapsin III gene silencing redeems alpha-synuclein transgenic mice from Parkinson's disease-like phenotype, Molecular Therapy (2022), https://doi.org/10.1016/j.ymthe.2022.01.021

no changes in the levels of Syn I and Syn II were observed in either the *substantia nigra* or *striatum* of the mice who received AAV-shSynIII injections, thus corroborating the specificity of Syn III gene silencing and supporting that the injection of the AAV-shNSC control vector did not perturb Syn III expression. To further confirm that Syn I levels in the nigrostriatal system were not increased by AAV-shSyn III injections, in spite of the significant improvement of Syn I mRNA expression induced by this AAV in the *substantia nigra* of SYN120 tg mice, we analyzed striatal Syn I immunolabeling, as Syn I strictly localizes in synaptic terminals in the adult brain.[18] In agreement with our wb data, we found that the C57BL/6J, C57BL/6JOlaHsd, and SYN120 tg mice injected with AAV-shSynIII exhibited a Syn I striatal immunolabeling that was comparable to that of their AAV-shNSC-injected littermates (Figure S1C). Syn I deficiency is known to contribute to the onset of an epileptic-like phenotype by altering the size of the SV readily releasable pool as well as the SV recycling rate and refilling in gamma-aminobutyric acid (GABA)ergic neurons.[19] However, Syn III knockout (ko) mice are not epileptic, likely because Syn III does not play a significant role in the control of GABAergic transmission, but rather regulates more specifically DA release in the adult brain.[8,18] Our findings support that Syn III gene silencing should not affect network excitability by indirectly affecting Syn I as the increase of Syn I mRNA expression induced by Syn III gene silencing in the SYN120 tg mice did not coincide with an increase of Syn I protein levels. This could be ascribed to differential changes in production and degradation rate that may enrich the mRNA levels but not protein expression.[20,21]

SYN120 tg mice injected with AAV-shSynIII exhibited reduced α-syn aggregation

We then evaluated α-syn aggregation in the *substantia nigra* and *striatum* of AAV-shSynIII- and AAV-shNSC-injected C57BL/6J, C57BL/6JOlaHsd, and SYN120 tg mice by performing thioflavin-S/α-syn double labeling (Figures 4A, 4B, S2A, and S2B). We previously reported that the overexpression of C-terminally truncated (1–120) α-syn results in the aggregation and deposition of the protein in the *substantia nigra* and *striatum* of these mice.[10,15,16] Here, we confirmed the presence of thioflavin-S/α-syn-positive inclusions in both the *substantia nigra* and *striatum* of AAV-shNSC-injected SYN120 tg mice (Figures 4A and 4B) but not in C57BL/6J and C57BL/6JOlaHsd controls (Figures S2A and S2B). This notwithstanding, the α-syn-positive neurons from SYN120 tg mice that were injected with AAV-shSynIII exhibited very faint thioflavin-S-positive signal. Consistently, the analysis of the images from SYN120 tg mice confirmed that those exposed to Syn III gene silencing exhibited a significant reduction of the thioflavin-S-positive area when compared with AAV-shNSC-injected littermates (Figures 4A and 4B). This supports a reduction of fibrillary α-syn aggregation in the brain of SYN120 tg mice exposed to Syn III gene silencing.

To corroborate this observation, we analyzed the detergent-insoluble striatal protein fractions reconstituted in UREA/SDS from SYN120 tg mice. We found that the samples from AAV-shSynIII-injected animals only exhibited a faint α-syn immunoreactivity, which instead was clearly detectable, as monomeric or high molecular weight forms, in the mice injected with AAV-shNSC (Figure 4C). This was confirmed by densitometric analysis of both α-syn monomer and high molecular weight bands in the UREA/SDS fractions (Figure 4C). No significant changes were observed in the radioimmunoprecipitation assay (RIPA)-soluble fraction of AAV-shSynIII-inoculated SYN120 tg animals when compared with AAV-shNSC littermates (Figure 4D).

Striatal sections were also stained with HS-68, a luminescent-conjugated oligothiophene, and α-syn, to evaluate possible changes in the conformation of α-syn aggregates as previously described.[22,23] Indeed, since the backbone of HS-68 is flexible, the binding and fluorescence emission of the molecule depends on the conformational properties of the aggregates.[24] By the analysis of the emission spectra of HS-68 in α-syn-immunolabeled striatal sections, we observed that AAV-shNSC-injected SYN120 tg mice exhibited a high fluorescence intensity (Figures 4E and S3A). Of note, the SYN120 tg animals exposed to Syn III gene silencing were found to exhibit a lower fluorescence intensity, supporting a decreased binding of HS-68 and thus a reduced presence of aggregates. When we then analyzed the ratio between the peaks at λ = 485 nm and λ = 570 nm as an index of the spectral distribution, we found that the spectrum of SYN120 tg mice injected with AAV-shNSC was blue shifted when compared to those of the SYN120 tg mice exposed to Syn III gene silencing (Figure 4F). These

Figure 2. Efficiency of Syn III gene silencing in the AAV-shSynIII-injected C57BL/6J, C57BL/6JOlaHsd, and SYN120 tg mice

(A) Representative images show Syn III and DAT-immunolabeling in the *striatum*. Graphs in middle panels show total Syn III-positive area (in μm^2) in the *striatum* of AAV-shSynIII-injected-mice when compared with the AAV-shNSC-injected mice. A significant reduction of Syn III-positive area in the AAV-shSynIII-injected C57BL/5J (***, –695 μm^2, $P < 0.001$), C57BL/6JOlaHsd (***, –942 μm^2, $P < 0.001$), and SYN120 tg mice (***, –1942 μm^2, $P < 0.001$) was detected. Graphs in right panels show the average size of Syn III-positive areas. Only SYN120 tg mice exhibited a significant decrease in this parameter (***, –0.33 μm^2, $P < 0.001$). Boxplots represent the distribution of the 75%, 50%, and 25% of the values. Whiskers indicate the upper and lower extreme of the dataset. Unpaired Welch's t test. $n = 4/5$ for each group. Scale bar: 20 μm. (B) Graphs show results of qRT-PCR results assessing the relative expression of Syn III, Syn II, and Syn I mRNA (expressed as fold changes in mRNA expression versus the mean mRNA levels of AAV-shNSC-injected C57BL/6J mice) in the *substantia nigra* of AAV-shSynIII- or AAV-shNSC-injected C57BL/6J, C57BL/6JOlaHsd, and SYN120 tg mice. A significant decrease of Syn III mRNA levels in the AAV-shSynIII-injected C57BL/6J (*, –0.56, $P < 0.05$), C57BL/6JOlaHsd (*, –1.93, $P < 0.05$), and SYN120 tg (*, –2.41, $P < 0.05$) animals with respect to their AAV-shNSC-injected littermates was detected. Syn III mRNA expression was increased in AAV-shNSC-injected C57BL/6JOlaHsd and SYN120 tg mice when compared to the C57BL/6J animals (*, +2.38, $P < 0.05$; *, +2.66, $P < 0.05$). No changes in Syn II mRNA expression were detected, while only SYN120 tg mice exhibited a marked increase in Syn I mRNA levels after the AAV-shSynIII injection when compared with the AAV-shNSC-injected littermates (**, +5.21, $P < 0.01$), with AAV-shNSC- and AAV-shSynIII-inoculated C57BL/6J mice (**, +5.76, $P < 0.01$; ***, +5.27, $P < 0.001$) and with AAV-shNSC-injected C57BL/6JOlaHsd (**, +5.10, $P < 0.01$). Data are expressed as mean ± SEM. Two-way ANOVA + Bonferroni's multiple comparisons test. $n = 4/5$ for each group.

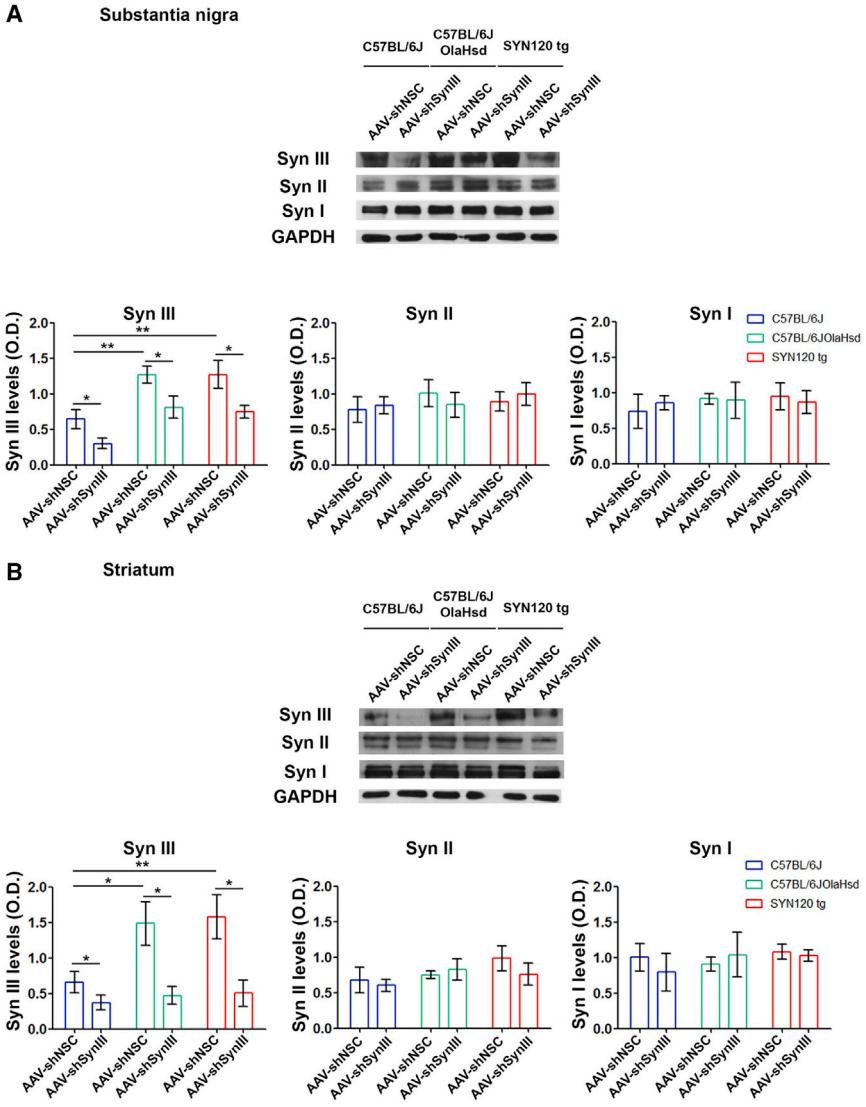

Figure 3. Western blot analysis evaluating the efficiency and specificity of Syn III silencing in the *substantia nigra* and *striatum* of AAV-shNSC- and AAV-shSynIII-injected mice

(A) Syn III protein levels were reduced in the AAV-shSynIII-injected *substantia nigra* of C57BL/6J (*, –0.34, $P < 0.05$), C57BL/6JOlaHsd (*, –0.46, $P < 0.05$), and SYN120 tg mice (*, –0.52, $P < 0.05$) when compared to AAV-shNSC-injected littermates. Please note the statistically significant increase of Syn III in C57BL/6JOlaHsd (**, +0.62, $P < 0.01$) and SYN120 tg mice (**, +0.63, $P < 0.01$) when compared to AAV-shNSC-injected C57BL/6J mice. No difference in Syn II or Syn I levels was observed. Data are expressed as mean ± SEM. Two-way ANOVA + Bonferroni's multiple comparisons test. $n = 6$ mice for each group. (B) The analysis of Syn III levels in the *striatum* showed a significant decrease in the AAV-shSynIII-injected C57BL/6J (*, –0.29, $P < 0.05$), C57BL/6JOlaHsd (*, –1.01, $P < 0.05$), and SYN120 tg mice (*, –1.07, $P < 0.05$) when compared to AAV-shNSC-injected littermates. Please note the statistically significant increase of Syn III in C57BL/6JOlaHsd (*, +0.82, $P < 0.05$) and SYN120 tg mice (**, +0.92, $P < 0.01$) when compared to AAV-shNSC-injected C57BL/6J mice. No differences were observed in Syn II or Syn I levels following Syn III gene silencing in the three mouse lines analyzed. Data are expressed as mean ± SEM. Two-way ANOVA + Bonferroni's multiple comparisons test. $n = 6$ mice for each group.

spectral differences support the occurrence of a change in aggregate conformation following Syn III gene silencing.

Finally, we also performed immunolabeling of aggregated α-syn on striatal sections from SYN120 tg mice by using an antibody (clone 5G4) that has been found to detect pathological aggregates in the brain of PD patients and animal models,[25,26] and we observed a significant reduction in immunopositivity in the animals exposed to Syn III gene silencing when compared with those injected with control AAV-shNSC (Figure S3B).

Gene silencing of Syn III rescues dopaminergic striatal fibers from degeneration in SYN120 tg mice

We previously showed that SYN120 tg mice do not present a significant TH-positive neuron loss in the *substantia nigra* that could justify a stereological-based count of these cells as a readout of a protective effect of Syn III gene silencing.[17] This notwithstanding, by exhibiting prominent striatal dopaminergic failure, SYN120 tg mice can be considered an ideal model recapitulating the initial neuropathological events driving nigrostriatal neurons deafferentation.[10,15,16] We thus evaluated whether the silencing of Syn III in SYN120 tg mice might efficiently counteract nigrostriatal fiber degeneration, a process occurring in the very early stages of PD[7]. Interestingly, a statistically significant loss of striatal TH-positive fibers was observed in the AAV-shNSC-injected SYN120 tg mice. Conversely, the decrease of TH-positive fibers was not detectable in the *striatum* of AAV-shSynIII-injected SYN120 tg littermates (Figure 5A) supporting that dopaminergic deafferentation was hampered by Syn III deletion.

These observations were corroborated by wb analysis of striatal protein extracts that confirmed that the AAV-shNSC-injected SYN120 tg mice displayed a significant decrease of TH levels when compared to C57BL/6J and C57BL/6JOlaHsd littermates (Figure 5B). Conversely, in the SYN120 tg mice injected with AAV-shSynIII we observed TH levels similar to the control C57BL/6J and C57BL/6JOlaHsd animals (Figure 5B). Of note, AAV-shSynIII injection did not alter TH levels in C57BL/6J or C57BL/6JOlaHsd mice, thus indicating that Syn III gene silencing does not affect the basal homeostasis of dopaminergic

Please cite this article in press as: Faustini et al., Synapsin III gene silencing redeems alpha-synuclein transgenic mice from Parkinson's disease-like phenotype, Molecular Therapy (2022), https://doi.org/10.1016/j.ymthe.2022.01.021

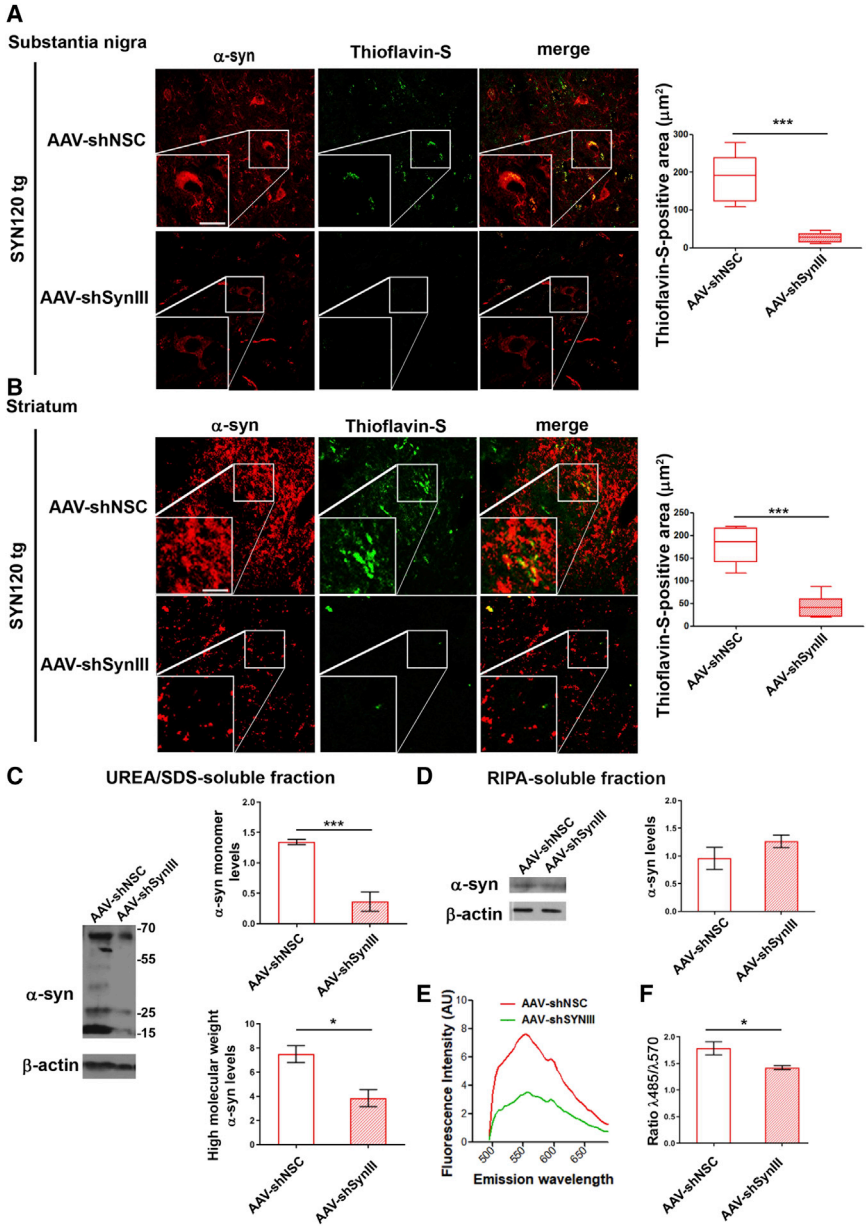

Figure 4. Gene silencing of Syn III prevents α-syn aggregation

(A) Representative images of thioflavin-S staining on α-syn-immunolabeled sections from the *substantia nigra* of AAV-shNSC or AAV-shSynIII-injected SYN120 tg mice. The graph shows the significant decrease of thioflavin-S-positive area in the animals exposed to AAV-shSynIII when compared to AAV-shNSC littermates (***, –161 μm^2, $P < 0.001$). Boxplots represent the distribution of the 75%, 50%, and 25% of the values. Whiskers indicate the upper and lower extreme of the dataset. Unpaired Welch's t test. $n = 5$ mice for each group. Scale bar: 20 μm. (B) Representative immunolabeling of α-syn coupled with thioflavin-S staining in the *striatum* of AAV-shNSC- or AAV-shSynIII-injected SYN120 tg mice. The graph is showing the significant decrease of thioflavin-S-positive area of AAV-shSynIII when compared to AAV-shNSC littermates (***, –136 μm^2, $P < 0.001$). Boxplots represent the distribution of the 75%, 50%, and 25% of the values. Whiskers indicate the upper and lower extreme of the dataset. Unpaired Welch's t test. $n = 5$ mice for each group. Scale bar: 20 μm. (C) Western blot analysis of the striatal UREA/SDS soluble fractions of AAV-shNSC- and AAV-shSynIII-injected SYN120 tg mouse brains revealed a statistically significant decrease of both monomeric and high molecular weight α-syn in the mice subjected to Syn III gene silencing (***, –0.98, $P < 0.001$ and *, –3.65, $P < 0.05$). Data are expressed as mean ± SEM. Unpaired Welch's t test. $n = 4$ mice for each group. (D) Western blot analysis of the striatal RIPA-soluble fractions of AAV-shNSC- and AAV-shSynIII-injected SYN120 tg mouse brains revealed no differences in the monomeric levels of α-syn. Data are expressed as mean ± SEM. Unpaired Welch's t test. $n = 4$ mice for each group. (E) Analysis of the spectral emission wavelength of the luminescent-conjugated oligothiophene HS-68 in striatal sections exposed to sequential α-syn-immunolabeling revealed with an Alexa 647 secondary antibody and HS-68 labeling. The SYN120 tg mice injected with AAV-shNSC exhibited a higher fluorescence intensity when compared to the AAV-shSynIII-injected littermates. $n = 3$ animals for each group. (F) The ratio between the peaks at $\lambda = 485$ nm and $\lambda = 570$ nm showed that the SYN120 tg mice injected with AAV-shNSC showed a blue shifted spectrum when compared the SYN120 tg mice exposed to Syn III gene silencing. Data are expressed as mean ± SEM. *$P < 0.05$, Unpaired Welch's t test. $n = 3$ animals for each group.

neurons (Figure 5B). This supports that the protective effect exerted by Syn III gene silencing on the striatal TH-positive fibers of SYN120 tg mice is likely consequent to the inhibition of α-syn aggregation. Finally, as TH is synthesized in neuronal soma and then transferred to axonal projections,[27] we analyzed TH expression levels in the *substantia nigra* by qRT-PCR. In line with the above described immunohistochemical and wb studies, we observed that TH expression was significantly reduced in the AAV-shNSC-injected SYN120 tg mice when compared to the C57BL/6J and C57BL/6JOlaHsd controls (Figure 5C).

Taken together, these observations indicate that, when performed in the very early phases of PD, Syn III gene silencing may hamper dopaminergic striatal deafferentation, which can act as the *primum movens* of the retrograde neuronal degeneration pattern characterizing this disorder.[7,28]

Syn III gene silencing reduces SV clustering in SYN120 tg mice

To evaluate the impact of the interplay between (1–120) α-syn and Syn III on the synapse organization, we performed a transmitted electron microscopy (TEM) ultrastructural analysis of the pre-synaptic

Please cite this article in press as: Faustini et al., Synapsin III gene silencing redeems alpha-synuclein transgenic mice from Parkinson's disease-like phenotype, Molecular Therapy (2022), https://doi.org/10.1016/j.ymthe.2022.01.021

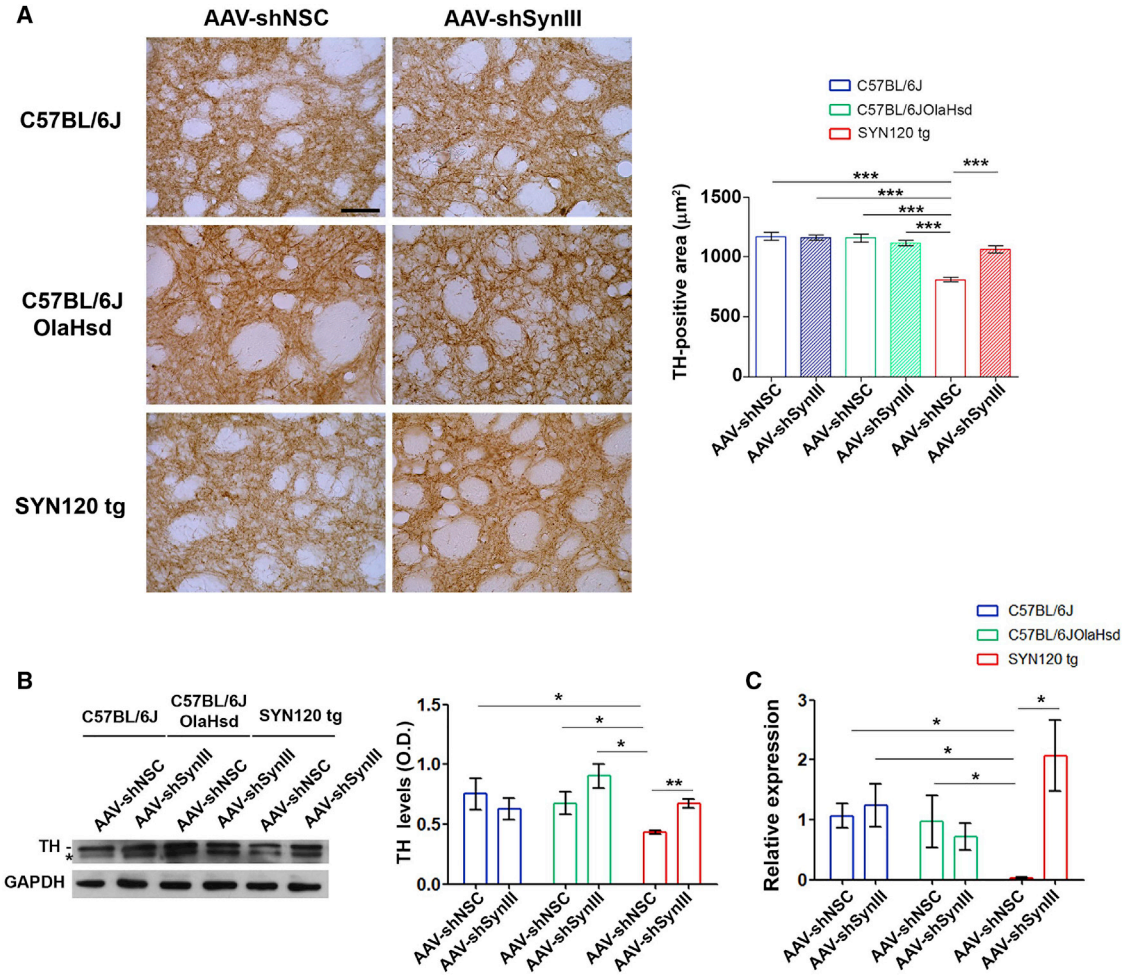

Figure 5. Syn III gene silencing reduces dopaminergic fiber loss in the *striatum* of SYN120 tg mice

(A) Representative images of TH-positive fibers in the *striatum* of AAV-shNSC- or AAV-shSynIII-injected C57BL/6J, C57BL/6JOlaHsd, and SYN120 tg mice. Graph shows densitometric analysis of TH-positive area (in μm^2) in the *striatum* of AAV-shNSC- or AAV-shSynIII-injected C57BL/6J, C57BL/6JOlaHsd, and SYN120 tg mice. AAV-shNSC-injected SYN120 tg mice showed a significant reduction of TH-positive area when compared to C57BL/6J (***, –355 μm^2, $P < 0.001$ for AAV-shNSC-injected mice; ***, –351 μm^2, $P < 0.001$ for AAV-shSynIII-injected mice), and C57BL/6JOlaHsd (***, –345 μm^2, $P < 0.001$ for AAV-shNSC-injected mice; ***, –307 μm^2, $P < 0.001$ for AAV-shSynIII-injected mice). TH-positive fiber loss in SYN120 tg mice was recovered by Syn III gene silencing (***, +242 μm^2, $P < 0.001$). Data are expressed as mean ± SEM. Two-way ANOVA + Bonferroni's multiple comparisons test. $n = 6$ for each group. Scale bar: 50 μm. (B) Western blot analysis showed that TH levels (expressed as optical density, O.D.) were reduced in the *striatum* of AAV-shNSC-injected SYN120 tg mice when compared to C57BL/6J (*, –0.32, $P < 0.05$) or C57BL/6JOlaHsd animals (*, –0.3, $P < 0.05$ for AAV-shNSC-injected mice; *, –0.47, $P < 0.05$ for AAV-shSynIII-injected mice). TH levels were significantly higher in the AAV-shSynIII-injected SYN120 tg mice when compared to AAV-shNSC-injected SYN120 tg littermates (**, +0.24, $P < 0.01$). Data are expressed as mean ± SEM. Two-way ANOVA + Bonferroni's multiple comparisons test. $n = 6$ for each group. Asterisk indicates a non-specific band that did not contribute to the quantification. (C) Graph shows qRT-PCR results for the relative TH expression (as fold changes of mRNA expression versus the mean mRNA levels of AAV-shNSC-injected C57BL/6J mice) in the *substantia nigra* of C57BL/6J, C57BL/6JOlaHsd, and SYN120 tg mice. In SYN120 tg mice TH mRNA expression was significantly increased by Syn III silencing (*, +2.03, $P < 0.05$). In the AAV-shNSC-injected SYN120 tg animals, TH expression was significantly lower than in C57BL/6J (*, –1.18, $P < 0.05$ for AAV-shNSC-injected mice; *, –1.21, $P < 0.05$ for AAV-shSynIII-injected mice), or C57BL/6JOlaHsd controls (*, –0.94, $P < 0.05$). Data are expressed as mean ± SEM. Two-way ANOVA + Bonferroni's multiple comparisons test. $n = 4/5$ for each group.

terminals in the *striatum* of each experimental group (Figure 6A). We observed that the C57BL/6JOlaHsd mice injected with AAV-shNSC exhibited a reduced density of SVs in striatal terminals when compared to the C57BL/6J littermates, thus supporting that the absence of α-syn impacts on SV organization (Figure 6B). This is in line with our previous studies showing a significant reduction of SVs per micrometer in the synaptic terminals of primary midbrain neurons from C57BL/6JOlaHsd animals[6]. Interestingly, the analysis of striatal synaptic terminals of the SYN120 tg mice injected with AAV-shNSC showed that the expression and aggregation of (1–120) α-syn on the C57BL/6JOlaHsd background resulted in a significant increase of SV density that was comparable to that of C57BL/6J mice (Figure 6B). In addition, we found that Syn III gene silencing did not affect SV density either in C57BL/6J or C57BL/6JOlaHsd

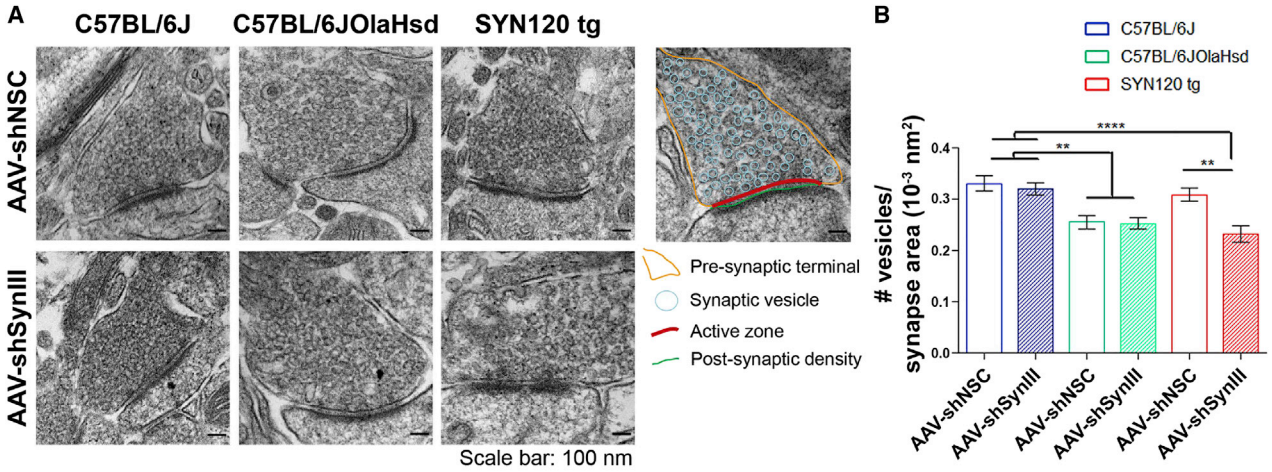

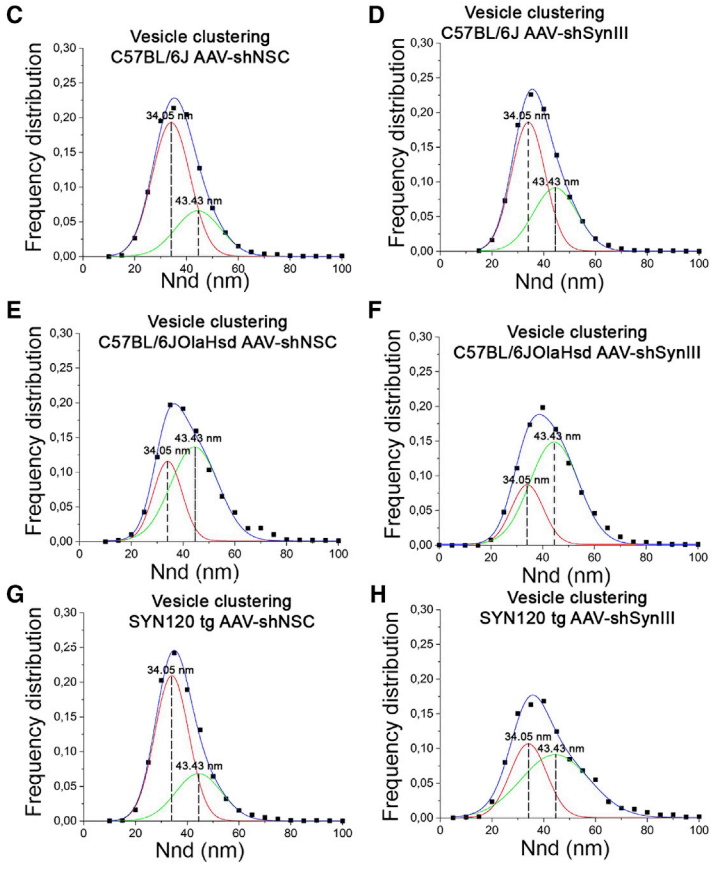

I

	C57BL/6J AAV-shNSC		C57BL/6J AAV-shSynIII		C57BL/6JOlaHsd AAV-shNSC		C57BL/6JOlaHsd AAV-shSynIII		SYN120 tg AAV-shNSC		SYN120 tg AAV-shNSC	
Area population 1 / Area population 2	Ratio	CI	Ratio	CI	Ratio	CI	Ratio	CI	Ratio	CI	Ratio	CI
	2.4	1.8-3.0	1.6	1.4-1.8	0.5	0.4-0.6	0.4	0.3-0.5	2.3	1.8-2.8	0.6	0.5-0.7

(legend on next page)

Please cite this article in press as: Faustini et al., Synapsin III gene silencing redeems alpha-synuclein transgenic mice from Parkinson's disease-like phenotype, Molecular Therapy (2022), https://doi.org/10.1016/j.ymthe.2022.01.021

mice, but it was able to significantly reduce the number of vesicles per synapse in the SYN120 tg mice at values comparable to those of C57BL/6JOlaHsd mice (Figure 6B). In light of our previous observations, and other studies supporting that α-syn aggregates cluster SVs,[6,29] the present findings suggest that the increased SV clumping observed in SYN120 tg mice injected with AAV-shNSC may be related to α-syn aggregate formation, while its decrease in the SYN120 tg mice exposed to Syn III gene silencing, could be the result of the reduction of the same process.

We then analyzed the frequency distribution of the nearest neighbor distance (NND) among vesicles. In this analysis, the multiple-peak Gaussian fit of each distribution (blue curves in Figures 6C–6H) revealed two main groups of SVs exhibiting the highest levels of goodness of the Gaussian fit (Figure S3J). Thus, these two groups represent the two main populations of SVs. These are population 1, that is indicated by the red peaks representing the SVs with mean distance between vesicle centroids of 34.05 nm, and population 2, that is indicated by the green peaks representing the SVs with mean distance between vesicle centroids of 43.43 nm, as in Figures 6C–6H. We found that in the C57BL/6J mice the mean distance between vesicle centroids was 34.05 nm for 70.9% of SVs following AAV-shNSC and for 61.0% of SVs following AAV-shSynIII injection, thus supporting that the majority of vesicles pertained to population 1. Interestingly, the NND of population 1 was almost comparable to the average diameter of SV in the AAV-shNSC- or AAV-shSynIII-injected C57BL/6J mice (Figures S3C and S3F). These findings support that in the synaptic terminals of these animals the vesicles were close to each other and that Syn III gene silencing did not significantly impact SV size and distribution. The Gaussian fit of the NND frequency distribution in the striatal synapses of C57BL/6JOlaHsd mice showed that the majority of vesicles (66.2% in the AAV-shNSC and 72.5% in the AAV-shSynIII) instead pertained to population 2 by exhibiting an inter-vesicle distance of about 43.43 nm (Figures 6E and 6F). This supported a reduced clustering of SVs in the C57BL/6JOlaHsd mice. Of note, the analysis of Gaussian fit further confirmed the above described improvement of vesicle density observed in the striatal synapses of SYN120 tg mice injected with AAV-shNSC versus their C57BL/6JOlaHsd littermates in the same experimental conditions. Indeed, while Syn III gene silencing was able to decrease vesicle clumping by rebalancing the majority of inter-vesicle distances (61.6%) of the striatal synapses of SYN120 tg mice at values comparable to population 2 as in the C57BL/6JOlaHsd mice (Figures 6E and 6F), in the AAV-shNSC-injected SYN120 tg littermates, 69.3% of SVs exhibited an inter-vesicle proximity comparable to that of population 1 as in the AAV-shNSC-injected C57BL/6J mice (Figures 6G and 6H). Remarkably, the analysis of the ratio between population 1 and population 2 in the different experimental groups confirmed the above observation (Figure 6I). Indeed, the ratio between population 1 and population 2 in the AAV-shSynIII-injected SYN120 tg mice was comparable to what observed in C57BL/6JOlaHsd mice, while the AAV-shNSC-injected littermates exhibited a ratio that was comparable to C57BL/6J mice (Figure 6I).

When we analyzed the mean diameter of SVs in the diverse mouse lines following either AAV-shNSC or AAV-shSynIII injection, we found that the C57BL/6JOlaHsd mice exhibited a higher SV diameter (38.3 ± 0.3 nm and 38.8 ± 0.3 nm) when compared with both C56BL/6J (35.6 ± 0.2 or 36.1 ± 0.2) and SYN120 tg mice (35.3 ± 0.1 and 35.9 ± 0.3) (Figures S3C–S3F). Since in the C57BL/6JOlaHsd animals the majority of SVs exhibited an NND of 43.43 nm, which is higher than the mean diameter of SVs (≅ 38 nm), we can conclude that the SVs of C57BL/6JOlaHsd mice did not exhibit a close proximity. On the same line, we can assume that in the SYN120 tg mice exposed to Syn III gene silencing, where the majority of SVs exhibited an NND of 43.43 nm and a mean diameter of ≅ 35 nm, the SVs were even more spaced than in C57BL/6JOlaHsd animals. Finally, no substantial difference in the frequency distribution of the vesicle distance from the active zone was observed in the three mouse lines analyzed in the presence or in the absence of Syn III (Figures S3G–S3I).

Syn III gene silencing restored the locomotor activity of SYN120 tg mice

We evaluated whether the protection from striatal dopaminergic fiber loss may coincide with a rescue of motility in SYN120 tg mice by using the beam walking and open field behavioral paradigms.

First, we assessed the time spent to travel the beam by C57BL/6J, C57BL/6JOlaHsd, and SYN120 tg mice (Figure 7A). When looking at animals injected with AAV-shNSC, we observed that the SYN120 tg mice spent more time to walk along the beam when compared to the C57BL6J and C57BL/6JOlaHsd littermates. Of note, AAV-shSynIII injection was able to significantly ameliorate the motor performances of SYN120 tg mice as supported by the

Figure 6. Syn III gene silencing reduces SV clustering in SYN120 tg mice

(A) Representative electron micrographs of pre-synaptic terminals for each experimental group. Scale bar: 100 nm. Image on the right is annotating the SVs (in light blue), the active zone (in red), the post-synaptic density (in green) within the presynaptic terminal (in yellow). (B) Quantification of vesicle density expressed as number of vesicles per synapse area (nm^2) in each experimental group. C57BL/6J AAV-shNSC: 60 synapses; C57BL/6JAAV-shSynIII: 60 synapses; C57BL/6JOlaHsd AAV-shNSC: 59 synapses; C57BL/6JOlaHsd AAV-shSynIII: 60 synapses; SYN120 tg AAV-shNSC: 60 synapses; SYN120 tg AAV-shSynIII: 63 synapses. Data are presented as mean ± SEM and analyzed by Kruskall-Wallis non-parametric test with Dunn's multiple comparison test (**$P < 0.01$, ****$P < 0.0001$). (C–H) Analysis of vesicle clustering by multiple-peak Gaussian fit of the frequency distribution of vesicle clustering in each experimental group in striatal synapses of C57BL/6J mice (C and D), C57BL/6JOlaHsd mice (E and F), and SYN120 tg mice (G and H). In the graphs, the red peaks represent population 1, which include the SV fitting under the curve with the median nearest neighbor distance (NND) = 34.05 nm, while the green peaks represent population 2, which includes the SV fitting under the curve with a median NND of 43.34 nm. The blue line indicates the cumulative fit of the NND of the two populations of SVs. Data are expressed in nanometers as frequency distribution of NND and fitted by multiple-peak Gaussian fit, comparing the AAV-shNSC and AAV-shSynIII conditions in each genotype. (I) The table shows the ratio between the area under the peak of population 1 and of population 2 and the respective 95% confidence interval (CI) of the AAV-shNSC and AAV-shSynIII-injected C57BL/6J, C57BL/6JOlaHsd, and SYN120 tg mice.

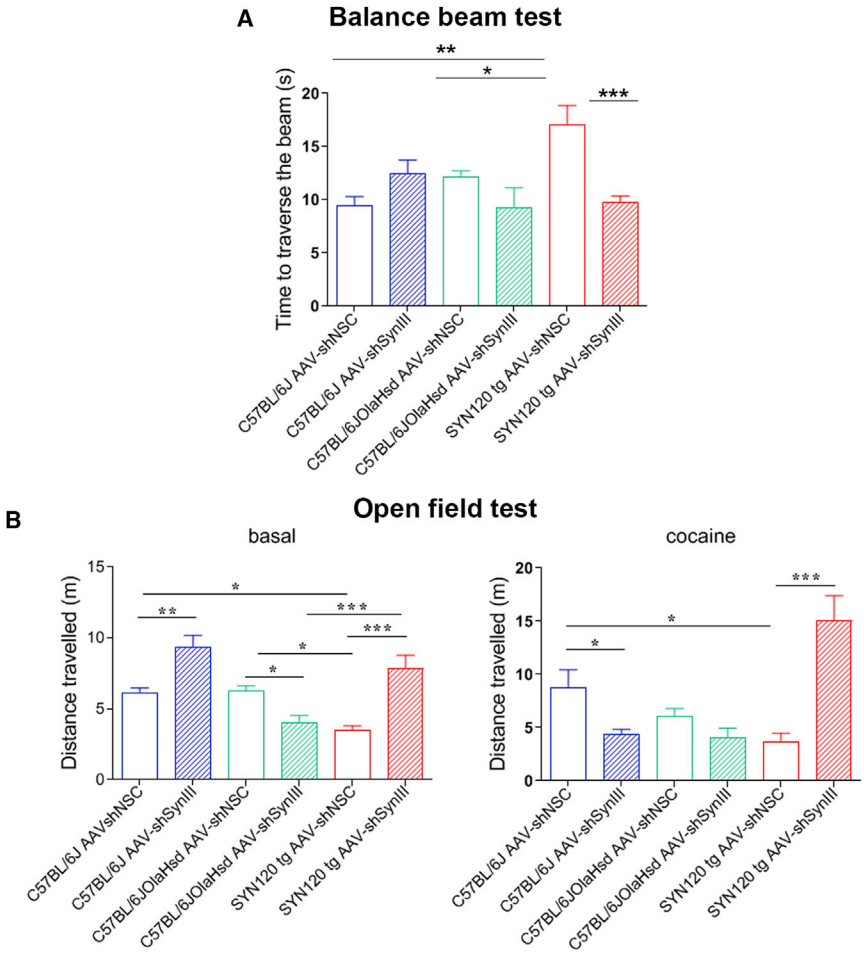

Figure 7. Syn III gene silencing abolished motility deficits in SYN120 tg mice

(A) Time spent to travel the beam by AAV-shNSC- or AAV-shSynIII-injected C57BL/6J, C57BL/6JOlaHsd, and SYN120 tg mice. The AAV-shNSC SYN120 tg mice spent more time than C57BL/6JOlaHsd (*, +4.06 s, $P < 0.05$) or C57BL/6J controls (**, +7.57 s, $P < 0.01$). Syn III deletion reduced the beam traveling time in SYN120 tg mice (***, –7.03 s, $P < 0.001$). One-way ANOVA + Newman-Keuls multiple comparisons test. $n = 10$ mice for each group. (B) Mean distance traveled by mice in the open field in basal condition (left graph) or following cocaine administration (right graph). AAV-shNSC-injected SYN120 tg mice exhibited reduced basal motility versus C57BL/6J (*, –2.64 m, $P < 0.05$) and C57BL/6JOlaHsd littermates (*, –2.78 m, $P < 0.05$). AAV-shSynIII injected C57BL/6J and SYN120 tg mice showed increased motility versus AAV-shNSC-injected littermates (**, +3.21 m, $P < 0.01$ and ***, +4.33 m, $P < 0.001$, respectively). AAV-shSynIII-injected C57BL/6JOlaHsd mice had reduced activity versus AAV-shNSC littermates (*, –2.31 m, $P < 0.05$) and AAV-shSynIII-injected SYN120 tg mice (***, –3.86 m, $P < 0.001$). AAV-shSynIII injection reduced cocaine response in C57BL/6J mice (*, –4.38 m, $P < 0.05$). SYN120 tg mice with AAV-shNSC injection showed decreased cocaine-induced locomotion versus C57BL/6J littermates (*, –5.08 m, $P < 0.05$), but this was recovered by Syn III deletion (***, +11.41 m, $P < 0.001$). C57BL/6JOlaHsd motility was not changed by cocaine administration. One-way ANOVA + Newman-Keuls multiple comparisons test. $n = 8/10$ mice for each group.

significant reduction in the time they employed to travel through the beam compared to their littermates injected with AAV-shNSC. However, AAV-shSynIII injection did not appear to influence the motor performances of control C57BL/6J and C57BL/6JOlaHsd mice, which exhibited a behavior similar to their respective AAV-shNSC littermates.

We then tested the motor abilities of C57BL/6J, C57BL/6JOlaHsd, and SYN120 tg mice injected either with AAV-shSynIII or AAV-shNSC in the open field test. In particular, we recorded the total distance traveled in basal condition and after an intraperitoneal (i.p.) acute administration of 10 mg/kg cocaine (Figure S4A). Indeed, we previously observed that aged SYN120 tg mice exhibit a significant reduction of cocaine-induced motility.[10] From our previous studies we knew that, although 16-month-old SYN120 tg mice show a compensatory increase of striatal DAT levels, they do not respond to DAT inhibitors as this protein is retained within the α-syn aggregates forming at synaptic terminals since 12 months of age.[10,30] Of note, DAT upregulation and the formation of α-syn/DAT complexes have been also reported to occur as an early pathological event in a synthetic human α-syn fibrils-based primate model of PD.[31] Consistently, we observed that spared α-syn/DAT complexes are still detectable in the *putamen* of postmortem brains of sporadic PD patients.[9,32]

We observed that the SYN120 tg mice injected with AAV-shSynIII were able to respond to cocaine administration, while their littermates injected with AAV-shNSC did not show cocaine-induced motor improvement (Figure S4A). Interestingly, cocaine administration reduced the locomotor activity of the C57BL/6J wt mice exposed to AAV-shSynIII-mediated gene silencing, and it did not induce a significant improvement of motility in the C57BL/6JOlaHsd mice in the same experimental condition when compared with their littermates injected with AAV-shNSC. Previous studies showed that Syn III ko mice display an increase in striatal dopamine release, thus supporting that the protein acts as a negative regulator on dopaminergic neurotransmission.[8] Of note, evidence showing that cocaine increases DA release by mobilization of a synapsin-dependent reserve pool, supports that the presence of Syn III allows the response to cocaine.[33] Consistently, the ability of cocaine to enhance DA release *in vivo* is reduced in Syn III ko mice.[8] Moreover, we previously demonstrated

Please cite this article in press as: Faustini et al., Synapsin III gene silencing redeems alpha-synuclein transgenic mice from Parkinson's disease-like phenotype, Molecular Therapy (2022), https://doi.org/10.1016/j.ymthe.2022.01.021

that α-syn and Syn III cooperatively regulate DA release and that C57BL/6JOlaHsd α-syn null mice exhibit an age-related variable motor response to acute cocaine administration in the open field likely as a result of the compensatory variation of Syn III and DAT levels occurring along aging.[6,10] The variable responses observed to cocaine administration in C57BL/6J, C57BL/6JOlaHsd, and SYN120 tg mice may thus be ascribed to Syn III gene silencing having a different effect depending on the presence or absence of either physiological full-length (fl) mouse α-syn or pathological human (1–120) α-syn expression.

By independently analyzing the total distances traveled either in basal condition or following cocaine administration (Figure 7B), we could appreciate that Syn III gene silencing was able to significantly improve basal motility in SYN120 tg mice, whose activity was comparable to that of the C57BL/6J mice injected with AAV-shSynIII. Conversely, the SYN120 tg mice injected with AAV-shNSC exhibited a significantly lower distance traveled when compared to the C57BL/6J mice in the same experimental condition. The AAV-shNSC-injected C57BL/6JOlaHsd mice showed a basal motility similar to that of C57BL/6J mice, but in contrast to what has been observed for these latter and for SYN120 tg mice, they did not exhibit locomotor activity changes following Syn III gene silencing. The SYN120 tg mice injected with the AAV-shSynIII also exhibited a higher response to cocaine when compared to their littermates receiving AAV-shNSC. In addition, when considering the animals injected with AAV-shSynIII, we also observed that cocaine administration reduced the motility of the C57BL/6J, whereas it did not perturb that of the C57BL/6JOlaHsd mice.

Lastly, we analyzed the overall DAT-immunopositive area as well as the size of DAT-immunopositive particles as an index of DAT distribution, in the *striatum* (Figure S4B). Striatal DAT-immunoreactivity in the AAV-shNSC- and AAV-shSynIII-injected C57BL/6J and C57BL/6JOlaHsd mice was similar. This notwithstanding, in line with our previous observations showing a marked α-syn aggregation-related redistribution and clustering of DAT immunoreactivity in the *substantia nigra* and *striatum* of SYN120 tg mice,[30] we found that in the AAV-shNSC-inoculated SYN120 tg mice the DAT-immunopositive signal showed areas of clumping (indicated by the arrows) (Figure S4B). Of note, DAT clumping was reduced in the SYN120 tg mice with Syn III gene silencing (Figure S4B). The analysis of striatal DAT-positive particles confirmed that in the AAV-shSynIII-injected SYN120 tg mice this parameter was comparable to both C5BL/6J and C57BL/6JOlaHsd mice, though the AAV-shNSC-injected SYN120 tg mice exhibited a significant increase in the size of DAT-immunopositive particles when compared with all the other mouse lines and to their littermates with Syn III gene silencing (Figure S4B). Interestingly, the α-syn aggregation-related redistribution of the DAT also occurs in the brain of sporadic PD patients and of non-human primates injected with pre-formed α-syn fibrils.[31,32] The analysis of total DAT-immunopositive area showed a significant decrease in the AAV-shNSC-injected SYN120 tg mice when compared with the C57BL/6J and C57BL/6JOlaHsd animals. In line with the above described recovery of TH-positive fibers following Syn III gene silencing in the SYN120 tg mice, these animals also exhibited a rescue of DAT-immunoreactivity. Together, these evidences support that Syn III gene silencing could allow the above described rescue of the response to cocaine in the SYN120 tg animals by enabling striatal dopaminergic fibers protection as well as a recovery of the proper DAT distribution at striatal dopaminergic terminals.

The SYN120 tg animals subjected to Syn III gene silencing exhibited recovery of DA release

Finally, we evaluated striatal DA release of freely moving C57BL/6J, C57BL/6JOlaHsd, and SYN120 tg animals injected either with AAV-shSynIII or AAV-shNSC by vertical microdialysis coupled to high-performance liquid chromatography (HPLC) (Figure 8A).

The results from the analysis of DA release appeared in agreement with the behavioral outcomes. Indeed, they confirmed that the SYN120 tg mice exposed to Syn III gene silencing displayed a significant increase of basal, depolarization-dependent (K^+-stimulated) and cocaine-induced DA release when compared to their littermates injected with AAV-shNSC. Conversely, the AAV-shNSC-injected SYN120 tg mice exhibited a significant reduction of DA release in basal as well as in K^+- or cocaine-stimulated condition when compared to C57BL/6J and C57BL/6JOlaHsd animals in the same experimental condition. In line with the data from the analysis of total distance traveled, supporting a reduction of motility following acute cocaine administration in the AAV-shNSC-injected C57BL/6J mice, we observed that these animals displayed lower DA release in response to this drug. In addition, we observed that the C57BL/6JOlaHsd mice exposed to Syn III gene silencing did not exhibit improvements in either basal, K^+-, or cocaine-stimulated DA release, suggesting that α-syn deficiency can affect the fundamental function of dopaminergic synaptic terminals and their capability to respond to depolarization or homeostatic changes in DA turnover.

DISCUSSION

The results of this study support that the AAV-mediated gene silencing of Syn III in the nigrostriatal system of a human α-syn tg mouse model of PD, at a pathological stage characterized by insoluble α-syn accumulation and dopaminergic synaptic dysfunction, exerts a disease-modifying effect. In particular, Syn III gene silencing reduced fibrillary insoluble α-syn aggregates in the *substantia nigra* and *striatum* of SYN120 tg mice, that were also protected from TH-positive fibers reduction in the *striatum*. The morphometric analysis of striatal pre-synaptic terminals highlighted that α-syn expression and aggregation differently impact SV organization. In particular, in the SYN120 tg animals, α-syn aggregation was associated with a marked increase in the density and clustering of SVs at striatal terminals with respect to what we observed in the littermates with similar genetic background, the C57BL/6JOlaHsd mice. Of note, Syn III deletion reduced SV clumping in the SYN120 tg mice, though it did not influence SV density and clustering in C57BL/6J or C57BL/6JOlaHsd mice. This supports that the decrease in SV clustering observed in the SYN120 tg mice occurs as a consequence of α-syn aggregates reduction.

Please cite this article in press as: Faustini et al., Synapsin III gene silencing redeems alpha-synuclein transgenic mice from Parkinson's disease-like phenotype, Molecular Therapy (2022), https://doi.org/10.1016/j.ymthe.2022.01.021

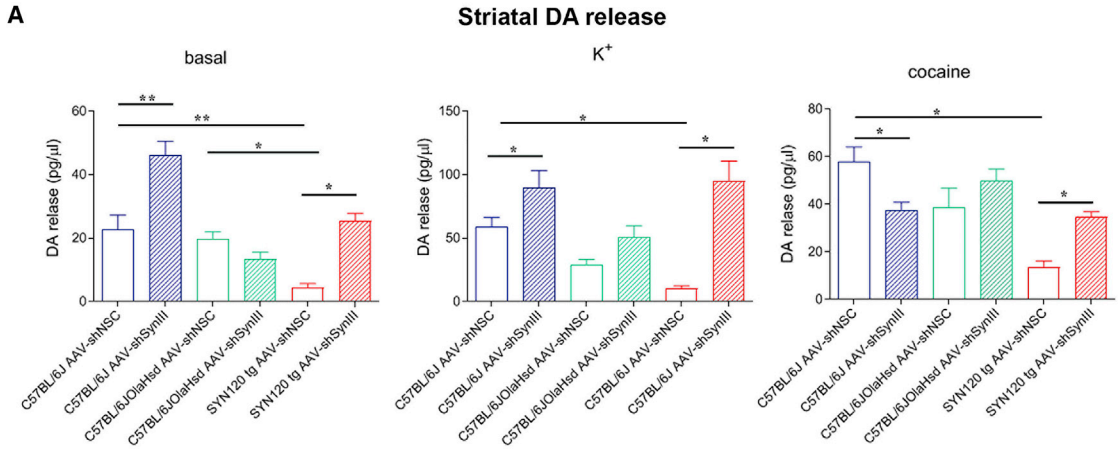

Figure 8. Syn III gene silencing restored striatal DA release in SYN120 tg mice

(A) Striatal DA release (pg/µL) as assessed by vertical microdialysis coupled with HPLC assays in basal condition (left graph) or following K^+ (central graph) or cocaine stimulation (graph on the right). AAV-shNSC-injected SYN120 tg mice exhibited a significant reduction in basal DA release when compared to AAV-shNSC-injected C57BL/6J (**, −18.42 pg/µL, $P < 0.01$) and C57BL/6JOlaHsd controls (*, −15.54 pg/µL, $P < 0.05$). AAV-shSynIII injection increased basal DA release in C57BL/6J (**, +23.40 pg/µL, $P < 0.01$) and SYN120 tg mice (*, +21.18 pg/µL, $P < 0.05$) when compared to their respective AAV-shNSC-injected littermates. Upon Syn III deletion, C57BL/6JOlaHsd mice exhibited a mild non-significant decrease in basal DA release. AAV-shSynIII-injected C57BL/6J showed increased K^+-stimulated DA release versus AAV-shNSC-injected littermates (*, +30.50 pg/µL, $P < 0.05$). SYN120 tg exhibited a significant decrease of DA release versus AAV-shNSC-injected C57BL/6J mice (*, −48.87 pg/µL, $P < 0.05$), that was rescued by Syn III deletion (*, +84.88 pg/µL, $P < 0.05$ versus AAV-shNSC SYN120 tg littermates). C57BL/6JOlaHsd had no change in K^+-stimulated DA release following Syn III deletion. AAV-shSynIII-injected C57BL/6J mice showed reduction of cocaine-induced DA release versus AAV-shNSC littermates (*, −44.17 pg/µL, $P < 0.05$). SYN120 tg mice exhibited a decrease of cocaine-stimulated DA release when compared to AAV-shNSC-injected C57BL/6J animals (*, −44.17 pg/µL, $P < 0.05$), but this was rescued by Syn III gene silencing (*, +21.11 pg/µL, $P < 0.05$ versus AAV-shNSC SYN120 tg littermates). Data are expressed as mean ± SEM. One-way ANOVA + Bonferroni's post-comparison test. $n = 6/8$ mice for each group.

Indeed, in this tg mouse line, insoluble α-syn aggregates in the nigrostriatal system start to develop around 6 months of age.[15] At 12 months of age, the SYN120 tg mice exhibit severe deficits in striatal DA release and synaptic pathology characterized by the accumulation of thioflavin-S-positive α-syn/Syn III co-aggregates and alterations in soluble NSF attachment protein receptor (SNARE) and DAT distribution.[16,30] Subsequently, the SYN120 tg mice develop overt motor deficits between 16 and 18 months of age,[10,15] though they do not exhibit a frank neuronal loss in the *substantia nigra*.[15]

Remarkably, by analyzing thioflavin-S and aggregated α-syn labeling, by using spectral analysis of HS-68 as well as through the quantification of UREA/SDS insoluble α-syn fractions, we observed that Syn III deletion could reduce the amount of α-syn aggregates. This was paralleled by a rescue of dopaminergic striatal functions in basal and depolarizing conditions or following the administration of cocaine, collimating with the improved basal and cocaine-stimulated motor abilities observed when the SYN120 tg mice with Syn III deletion were compared to their littermates injected with AAV-shNSC. Our behavioral and functional studies also showed that C57BL/6J and C57BL/6JOlaHsd mice exhibited different responses to Syn III gene silencing. In particular, the C67BL/6J animals injected with AAV-shSynIII exhibited an enhancement of DA release and motility in basal condition, but they did not display a normal response to cocaine. This is in line with evidence supporting that Syn III acts as a negative regulator of DA release in the *striatum* and that its deletion reduces cocaine-dependent DA release.[8,33] In the C57BL/6JOlaHsd mice, we did not observe differences in motility or DA release following Syn III deletion. Both the AAV-shNSC and AAV-shSynIII-injected C57BL/6JOlaHsd mice exhibited the same open field motility profile that we previously observed for their non-injected littermates,[10] which lost the ability to respond to cocaine administration at 16 months of age. The fact that Syn III does not perturb DA release and motility in the absence of α-syn reinforces that these proteins exert a cooperative control of dopaminergic neurotransmission.[6] Interestingly, following Syn III gene silencing in the SYN120 tg mice, we observed an opposite behavior with respect to C57BL/6J mice upon cocaine stimulation, as the SYN120 tg mice exhibited an improvement of DA release. This was probably ascribed to the occurrence of a differential synaptic homeostatic response to Syn III deletion in the two mouse lines. Indeed, at the time of AAV injections (12 months of age) the SYN120 tg mice already exhibit human (1–120) α-syn aggregation-related pathological alterations and severe dysfunctional problems,[10,16] which associate with a reduction of functional DAT, as the protein is retained within α-syn aggregates.[30,32] It is thus feasible that the reduction of α-syn aggregation observed following Syn III gene silencing in the SYN120 tg mice may have allowed a restoration of DAT membrane transportation, thus enabling cocaine response.

Although Syn III deletion was able to affect striatal DA release and motility of C57BL/6J and C57BL/6JOlaHsd mice, the results from our morphological TEM studies on striatal terminals support that it

Please cite this article in press as: Faustini et al., Synapsin III gene silencing redeems alpha-synuclein transgenic mice from Parkinson's disease-like phenotype, Molecular Therapy (2022), https://doi.org/10.1016/j.ymthe.2022.01.021

did not significantly impinge on SV size and organization in these mouse lines. This is in agreement with our previous observations in the brain of young 4-month-old Syn III ko mice that exhibited a number of SVs at the active zone and an SV diameter comparable to C57BL/6J wt mice.[11] In this previous study, we did not address SV clustering, but we observed that AAV-mediated human fl α-syn overexpression in the nigrostriatal system induced a significant reduction in the number of SVs at the active zone while increasing SV diameter.[11] These features were instead not detected in the SYN120 tg mice. This notwithstanding, we found that (1–120) α-syn aggregation was associated with an improvement of the density and clustering of SVs when compared to what observed in the C57BL/6JOlaHsd mice, which represent their genetic background, and this effect was recovered upon Syn III deletion. These observations indicate that by hampering SV motility, α-syn aggregation in the SYN120 tg mice can induce nigrostriatal neurons dysfunction and initiate axonal degeneration. Indeed, α-syn aggregation is significantly reduced following Syn III deletion in the SYN120 tg mice, and this results in the abolishment of SV clumping, recovery of DA release and motility, and reduced TH-positive fibers loss in the *striatum*.

Since the C57BL/6JOlaHsd α-syn null mice exhibited a significant increase of SV diameter when compared with C57BL/6J wt mice, it may be feasible that the increase of SV diameter and decrease in active zone SVs previously detected in the AAV-based human fl α-syn overexpression mouse model, which was produced on a mouse C57BL/6J genetic background, was ascribed to the loss of function of mouse endogenous α-syn, occurring as a consequence of its fast recruitment into pathological aggregates with human α-syn.[11] This sounds in agreement with previous studies on primary hippocampal neurons from mice overexpressing human eGFP-tagged fl human α-syn under the guidance of the platelet-derived growth factor promoter, where aggregation of the protein was found to affect the size and clustering of SVs.[34] In the light of evidence supporting that α-syn is a key regulator of membrane curvature,[35] our present findings showing that the SYN120 tg mice exhibit an SV diameter comparable to C57BL/6J mice suggest that the human (1–120) non-aggregated α-syn fraction still compensates for the absence of endogenous mouse α-syn in the C57BL/6JOlaHsd genetic background, even when the tg animals exhibit marked insoluble aggregates deposition and dysfunction. The differences in the speed and severity of α-syn aggregates deposition and PD-like phenotype development, in concert with the distinct genetic backgrounds (C57BL/6J versus C57BL/6JOlaHsd), could instead explain the diverse distribution of active zone vesicles observed between the AAV-based human fl α-syn overexpressing mice and the SYN120 tg mice.

Remarkably, our findings supporting that Syn III gene silencing does not impinge on α-syn-mediated regulation of SV size or on the number of active zone SVs in the SYN120 tg mouse line, or in control mice, support that the manipulation of this protein would not perturb this specific function of α-syn. Consistently, Syn III ko mice exhibit comparable SV size and numbers at the active zone when compared to C57BL/6J wt mice in basal condition.[11] This notwithstanding, a significant increase in the number of SVs at the active zone following human fl α-syn overexpression in Syn III ko animals was observed.[11] Since in the Syn III ko mice α-syn aggregation is hampered, we can speculate that the improvement in SVs at the active zone was related to the additional effect of endogenous mouse α-syn coupled with the overexpression of human fl α-syn, which would both promote the docking of SVs to the plasma membranes in line with previous findings.[36]

It has been recently shown that α-syn plays a crucial role in activity-dependent dopaminergic neurons plasticity, as it facilitates DA release when triggered by short repeated burst, while it depresses the same process upon prolonged burst activity.[5] In the light of our results, it thus sounds feasible that both these events may be compromised by the deposition of α-syn aggregates, which can clump and block SVs. However, our findings support that Syn III gene silencing may be able to rescue both the above-cited modality of α-syn-mediated control of DA transmission.

Of note, we recently found that similarly to Syn III gene silencing, the AAV-mediated expression of the synaptic chaperone cysteine string protein α (CSPα), a protein controlling SV exocytosis and which is reduced by α-syn pathological deposition, is also able to rescue α-syn aggregation and DA release in the nigrostriatal system of 12-month-old SYN120 tg mice.[37] This observation, when coupled to the present findings, support that by changing the levels of proteins that are known to cooperate with α-syn at synaptic terminals,[4] we can impact stability of aggregates.

Although our findings appear to suggest that similarly to CSPα overexpression, Syn III deletion could affect α-syn aggregation by regulating SV motility and exocytosis, the absence of a clear alteration of SV distribution and clustering or in the number of active zone vesicles following Syn III removal in C57BL/6J and C57BL/6JOlaHsd mice rules out this possibility. Our previous observations on the presence of Syn III in fibrils extracted from postmortem brains of sporadic PD patients showing α-syn/Syn III co-pathology[32] rather support that Syn III may be directly and actively involved in α-syn fibrillation and stabilization of α-syn fibrils.

Interestingly, a functional interaction between α-syn in a low aggregation propensity α-helical state and Syn III is necessary for the promotion of Syn III-dependent motor response to acute MPH administration in SYN120 tg mice.[10] This supports that a dual role for Syn III in physiological and pathological α-syn regulation may be envisaged. On the one hand, Syn III would bind α-syn fibrils, thus allowing aggregate stabilization. On the other hand, functional Syn III would interact with monomeric α-helical α-syn thus promoting DA release. It may thus be feasible that by recruiting Syn III and promoting its interaction with this α-helical monomeric α-syn conformation, MPH could reduce in parallel the binding of Syn III to fibrils, thus mimicking the effect of Syn III deletion. Therefore, although we envisage that the gene silencing of Syn III does not

represent a feasible approach for clinical translation, the fact that the protein can be pharmacologically targeted[14] opens the way toward the development of novel agents modulating its function. Studies aimed at clarifying the features of pathological and functional α-syn/Syn III interaction and at developing novel specific Syn III-active compounds are ongoing.

Collectively, these findings indicate that Syn III plays a key role in maintaining or stabilizing α-syn aggregates and that its gene silencing in an established mouse model of PD at pathological stage reduces pathological α-syn deposition and striatal dopaminergic fibers loss and rescues DA release and motor functions. We thus foresee that therapeutic strategies targeting Syn III could be of help in the context of PD or other synucleinopathies.

MATERIALS AND METHODS

Animals

C57BL/6J mice (Charles River, Wilmington, MA), C57BL/6JOlaHsd carrying a spontaneous deletion of α-syn gene (Harlan Olac, Bicester, UK), and SYN120 tg mice[15] were used. Mice were bred at the animal house facility at the Department of Molecular and Translational Medicine of University of Brescia, Brescia, Italy. Animals were maintained under a 12-h light–dark cycle at a room temperature (rt) of 22°C and had *ad libitum* food and water. All experiments were made in accordance to Directive 2010/63/EU of the European Parliament and of the Council of September 22, 2010, on the protection of animals used. All experimental and surgical procedures conformed to the National Research Guide for the Care and Use of Laboratory Animals and were approved by the Animal Research Committees of the University of Brescia (Protocol Permit 719/2015-PR). All efforts were made to minimize animal suffering and to reduce the number of animals used.

Animal surgery

Twelve-month-old SYN120 tg male mice were bilaterally injected in the *substantia nigra* with either AAV-shSynIII or AAV-shNSC at a concentration of 10^{12} genome copies/mL. Both AAV-shSynIII and AAV-shNSC were serotype 2/6 and also drove the expression of an eGFP reporter under the guidance of the cytomegalovirus (CMV) promoter, while shSynIII or shNSC expression was driven by the U6 promoter (Vector biolabs, Malvern, PA, USA).[10] Briefly, animals were anesthetized and placed in a stereotactic head frame (Stoelting, IL, USA). After making a midline incision of the scalp, a hole was drilled in the appropriate location for *substantia nigra* at the left and right side of the skull. Two microliters of AAV-shSynIII or AAV-shNSC were injected at a rate of 0.2 μL/min with a 33-gauge needle on a 10 μL Hamilton syringe at the following coordinates: antero-posterior – 3.70; medio-lateral + and – 1.50; dorsal-ventral – 3.9 relative to bregma.[38] The needle was left in place for an additional 5 min before being slowly retracted from the brain. All the AAV-shSynIII- and AAV-shNSC-injected mice were analyzed 4 months after the AAV injections.

Double immunofluorescence staining

Mice were anesthetized by i.p. injection of chloral hydrate (400 mg/kg) (Sigma-Aldrich, St. Louis, MO, USA) and perfused transcardially by using a 4% paraformaldehyde (PFA) Immunofix solution (Bio-optica, Milan, Italy). After 4 h of post-fixation in 4% PFA, brains were incubated in a solution of PBS with high salt concentration (NaOH 200 mM, NaH_2PO_4 245 mM, NaCl 0.9%) containing 18% sucrose for at least 24 h, then 25-μm coronal sections were cut with a cryostat (Leica Biosystems, Milan, Italy) and stored in 60% glycerol. Only in the case of the immunolabeling with the aggregated α-syn antibody (5G4), slices were subjected to antigen retrieval for 5 min in sodium citrate buffer (10 mM, pH 6) at 95°C.

After permeabilization in 20% methanol and 0.3% Triton X-100 in PBS 0.1 M, the free-floating sections were incubated for 1 h at rt in blocking solution (2% v/v normal goat serum [NGS], 3% w/v BSA, 0.3% Triton X-100 in PBS 0.1 M), and then with the primary antibody diluted in blocking solution overnight (o.n.) at 4°C. The following day, sections were washed with 0.3% Triton X-100 PBS 0.1 M and incubated with the fluorochrome-conjugated secondary antibody in 0.3% Triton X-100 PBS 0.1 M plus 1 mg/mL BSA for 1 h at rt. After three washes in 0.3% Triton X-100 PBS 0.1 M, sections were incubated for 2 h at rt with the second primary antibody, followed by incubation for 1 h at rt with the appropriate secondary antibody. Lipofuscin was quenched with TrueBlack Lipofuscin Autofluorescence Quencher (Biotium, Fremont, CA), then slices were mounted onto glass slides using Vectashield (Vector Laboratories, Burlingame, CA) and analyzed by confocal microscopy.

Thioflavin-S staining

Mouse brain sections were incubated with 0.05% thioflavin-S (Sigma-Aldrich) dissolved in 50% ethanol for 8 min and subsequently washed in 80% ethanol to eliminate unspecific dye residues. Sections were then incubated in blocking buffer before immunostaining with the antibody against α-syn, mounted on glass slides, and analyzed by confocal microscopy. For thioflavin-S detection, images were acquired with laser excitation set between 350 and 400 nm. For image analysis of thioflavin-S-positive area a total of eight images taken from eight serial sections at 80-μm interval from the *substantia nigra* and *striatum* were analyzed for each animal.

HS-68 oligothiophene/α-syn double labeling and spectral analysis

The synthesis of HS-68 has been described.[24] Mouse brain sections were incubated with HS-68 for 30 min at rt as previously described.[22] Sections were then incubated in blocking buffer before immunostaining with the antibody against α-syn (Syn1, Beckton Dickinson, Milan, Italy), revealed by using an Alexa 647-conjugated secondary antibody (Jackson Immunoresearch, Pennsylvania, USA), and mounted on slides. The double-positive aggregates were analyzed by averaging 10 regions of interest for each of the eight images acquired from each of the eight serial sections selected at 80-μm interval for each animal. In particular, emission spectra were acquired with laser excitation set at 458 nm by using a Zeiss LSM880 microscope (Carl Zeiss,

Milan, Italy). The mean of the HS-68 spectral values of each animal was plotted on a graph.

Confocal microscopy

The slides were observed by an LSM 880 Zeiss confocal laser microscope with the laser set on λ = 405–488–543–633 nm and the height of the sections scanning = 1 μm. Images (512 × 512 pixels) were then reconstructed using ZEISS ZEN Imaging Software (Carl Zeiss).

Quantitative real-time PCR

Total RNA was extracted from the *substantia nigra* of C57BL/6J, C57BL/6JOlaHsd, and SYN120 tg mice using an RNA extraction kit (RNeasy Mini Kit, Qiagen, Hilden, GE) according to the manufacturer's instructions. Two μg of RNA was retrotranscribed by using QuantiTect Reverse Transcription Kit (Qiagen) according to the manufacturer's instructions. The qRT-PCR was performed by using SYBR Green Master Mix (Applied Biosystems, Foster City, USA) and the following primers pairs: *Syn III* for aaatcagcatcaccccaccc, *Syn III* rev gccttggcctcatcttcact; *Syn II* for ctcaacaagtcgcagtccct; *Syn II* rev agaggctggcaaaggacttc; *Syn I* for tcctcctgctcaacaacgac; *Syn I* rev cggtccaaggccagaaagat; *TH* for tgaaggaacggactggcttc; *TH* rev gagtgca taggtgaggaggc; *GAPDH* for tcaacagcaactcccactctt, and *GAPDH* rev ccagggtttcttactccttgg.

The ViiA7 Real-time PCR system (Life Technologies, Grand Island, NY, USA) was used for 40 cycles of 95°C for 15 s and 60°C for 1 min. mRNA expression was normalized to GAPDH gene expression. Each experimental condition was analyzed in triplicate and the resulting data were averaged and subjected to statistical analysis. The mean value of the AAV-shNSC-injected C57BL/6J controls from each triplicate was used to normalize all the samples. Each experimental value is standardized to the control mean value.

Western blot analysis

Fresh frozen tissues from the *substantia nigra* and *striatum* were collected from mouse brains after cervical dislocation. Total proteins were extracted with RIPA buffer made of 50 mM Tris-HCl (pH 7.4), 150 mM NaCl, NP-40 1%, sodium deoxycholate 0.1%, SDS 0.1%, 1 mM NaF, 1 mM $NaVO_4$ plus complete protease inhibitor mixture (Roche Diagnostics, Mannheim, Germany). Protein concentration in the samples was measured by using the Bio-Rad DCTM protein assay kit (Bio-Rad Laboratories, Milan, Italy). Equal amounts of proteins (30 μg) were run in 10% polyacrylamide gels and transferred onto polyvinylidene fluoride membrane. Densitometric analysis of the bands was performed by using FIJI software, and all bands were normalized to GAPDH levels as a control of equal loading of samples in the total protein extracts. For densitometry analysis of bands, each experimental condition was performed in triplicate and the resulting data were subjected to statistical analysis.

Detergent-insoluble α-synuclein extraction

Alpha-synuclein insoluble aggregates were extracted from *striatal* fresh tissues, after homogenization in tris-buffer saline+ (TBS+) solution composed of 50 mM Tris-HCl (pH 7.4), 175 mM NaCl, 5 mM EDTA, 0.1 mM PMSF, 1 mM *N*-ethyl-maleimide, plus complete protease inhibitor mixture (Roche Diagnostics) and centrifugation at 50,000 g for 30 min at 4°C.[15] Pellets were resuspended in TBS+ solution plus 1% Triton X-100 and centrifuged at 50,000 *g* for 30 min at 4°C and then reconstituted in RIPA buffer and subjected to a further centrifugation. The final pellets were resuspended in 8 M urea plus 5% SDS and loaded on 10% polyacrylamide gel. For densitometry analysis of bands, each experimental condition was performed in triplicate and the resulting data were averaged and subjected to statistical analysis. All bands were normalized to beta-actin levels as a control of equal loading of samples in the UREA/SDS protein extracts. Three animals for each group were analyzed.

Immunohistochemistry (IHC) and bright-field microscopy

Mice were anesthetized as described above. Sections of the *striatum* and *substantia nigra* were permeabilized with 20% methanol and 5% H_2O_2, washed and incubated with primary antibody o.n. at 4°C. The following day, sections were washed and incubated with biotinylated secondary antibody for 45 min at rt. This was followed by gentle washing, and incubation with avidin-biotin complex (ABC kit, Vector Laboratories) at rt for 45 min and staining visualized with 3,3′-diaminobenzidine (DAB) staining (Vector Laboratories) for 5 min. Finally, sections were washed, dehydrated, mounted with Vectamount mounting medium (Vector Laboratories), and were acquired by using an inverted light/epifluorescence microscope (Olympus IX50; Olympus, Milan, Italy).

Antibodies

Primary and secondary antibodies and their working dilutions are summarized in Table 1.

Image analysis of eGFP/TH-positive signal in the *substantia nigra*

Striatal TH- and eGFP-positive area was examined from digitized images using FIJI software as previously described.[11] Five sections from each mouse were analyzed by examining an average of five fields per section. The area of colocalization between TH and eGFP was quantified by using Zen software (Carl Zeiss). The area of TH/eGFP colocalization was then normalized on the total TH-positive area for each field to estimate the percent amount of TH-immunoreactivity exhibiting eGFP signal. The values deriving from the different fields analyzed for each section were averaged, and the resulting values for the different animals were plotted and subjected to statistical analysis.

Image analysis of Syn III-, syn I-, DAT-, or aggregated α-syn-immunopositive area in the *substantia nigra* and *striatum*

For the quantification of the immunoreactivity for Syn III, Syn I, DAT, or aggregated α-syn as recognized by the 5G4 antibody, the acquisition parameters during confocal imaging were maintained constant for all the images acquired. Brains (10 sections from each mouse, two every 150 μm) were analyzed by examining the whole area of the *substantia nigra* within a virtual standard grid composed of eight fields. The total Syn III-positive or 5G4-positive area within the grid was estimated by using the FIJI software. The mean Syn III-positive area was calculated by averaging the values of the ten grids

Please cite this article in press as: Faustini et al., Synapsin III gene silencing redeems alpha-synuclein transgenic mice from Parkinson's disease-like phenotype, Molecular Therapy (2022), https://doi.org/10.1016/j.ymthe.2022.01.021

Table 1. List of the primary and secondary antibodies used for the study and of their working dilutions

Antibody	Manufacturer	Host species	Working dilution	
			wb	IHC
α-syn (5G4, MABN389)	Cell Signaling	Rabbit		1:400
α-syn (syn1, 610787)	BD	Mouse	1:1,000	1:500
β-actin (251001)	Synaptic System	Mouse	1:10,000	
DAT (sc-32258)	Santa Cruz	Rat		1:500
GAPDH (G8795)	Sigma-Aldrich	Mouse	1:7,000	
GFP (ab183734)	Abcam	Rabbit		1:500
Syn III (106,303)	Synaptic System	Rabbit	1:3,000	1:600
Syn II (106,203)		Rabbit	1:3,000	
Syn I (106,103)		Rabbit	1:3,000	1:600
TH (AB152)	Millipore	Rabbit	1:2000	1:600
anti-mouse IgG Cy3-conjugated	Jackson ImmunoResearch	Goat		1:1,000
anti-rabbit IgG Cy3-conjugated		Goat		1:1,000
anti-rat IgG Cy3-conjugated		Goat		1:1,000
anti-rat IgG Alexa 647-conjugated		Goat		1:800
anti-rabbit IgG Alexa 647-conjugated		Goat		1:1,000
biotinylated anti-rabbit IgG	Vector Laboratories	Goat		1:1,000
anti-rabbit IgG-HRP	Promega	Goat	1:3,000	
anti-mouse IgG-HRP		Goat	1:3,000	

analyzed for each animal in the different experimental groups. The optical density of the striatal Syn III- or Syn I- or DAT-positive area and the average size of Syn III- or DAT-positive particles from digitized images acquired by confocal microscopy were examined by a researcher blind to the experimental conditions by using FIJI software. Eight fields per section were analyzed. The threshold setup for FIJI was fixed between 30 and 150.

Analysis of TH-positive fibers density in the *striatum* and *substantia nigra*

The optical density of striatal TH-positive area was examined from digitized images using FIJI software as previously described.[11] Five sections from each mouse were analyzed by examining an average of ten fields per section. Data from TH analysis were expressed as the positive area in each sample.

The TH-positive neurons in the *substantia nigra* were analyzed by examining digitized images using FIJI software. Six sections from each mouse (30 μm thick) were acquired every 150 μm in a rostro-caudal extension. The optical density of nigral TH-positive area from each image was summed and averaged by examining six mice for each condition. Data from nigral TH-positive area were expressed as percent changes versus the AAV-shNSC-injected C57BL/6J control mice.

Beam walking test

The time spent to traverse the beam in the balance beam test was assessed as previously described.[39] The beam, 2.5 cm width and 1 m length, was placed at 25 cm height ending into the animal's home cage. A first day of training was performed for a total of four trials every 30 min. The animal was trained to traverse the entire length of the beam by placing it at the beginning of the beam and moving the home cage in close proximity to the animal to encourage the movement forward along the beam. The following day the time taken to cross the beam was measured. The time was evaluated from when the mouse began to move forward and ended when the first forepaw was placed outside the beam.

Open field behavioral tests

Acute locomotor activity of C57BL/6J, C57BL/6JOlaHsd, and SYN120 tg was assessed using the automated ANY-maze video tracking system (Stoelting, Wood Dale, IL, USA) according to previously described protocols.[6] The total distance traveled was recorded automatically with ANY-maze behavioral tracking software (Stoelting) in the open-field arena (50 × 50 cm^2) and data were analyzed in 14 trials of 2.5 min each. Mice were gently placed in the arena and were allowed to explore freely for 5 min before starting the test. After 10 min of registration in basal condition, mice received an i.p. injection of cocaine (10 mg/kg, dissolved in normal saline 0.9%) (Tocris, Bristol, UK) to evaluate their ability to respond to a stimulus promoting DA neurotransmission. All the experiments were conducted during daylight hours.

Vertical microdialysis and HPLC assays

Extracellular DA levels were measured in the *striatum* of C57BL/6J, C57BL/6J, and SYN120 tg mice 4 months after the injection of AAV-shSynIII or AAV-shNSC by using vertical microdialysis coupled to HPLC as previously described.[16] Mice were anesthetized with tiletamine-zolazepam (75 mg/kg i.p.) before being placed in a stereotaxic frame. After sagittal cutting, the overlying skin was retracted, folded away, and a hole drilled at the level of the right dorsal *striatum* (antero-posterior + 0.6; medio-lateral + 1.8; dorsal-ventral – 2.1 from the bone); all coordinates[38] were taken over the bone and referred to bregma, with bregma and lambda on a horizontal plane. A microdialysis CMA/7 guide cannula (CMA Microdialysis, Stockholm, Sweden) was then gently inserted through the hole using the micromanipulator of the stereotaxic instrument. The cannula was secured with acrylic dental cement and the skin sutured. Mice were housed with free access to food and water to recover from surgery (one mouse per cage). The following day, a CMA/7 microdialysis probe was inserted into the guide cannula and perfused at a constant flow rate (2 μL/min) with artificial cerebrospinal fluid (ACSF) containing 140 mM NaCl, 7.4 mM glucose, 3 mM KCl, 0.5 mM $MgCl_2$, 1.2 mM $CaCl_2$, 1.2 mM Na_2HPO_4, 0.3 mM NaH_2PO_4 (pH 7.4). The dialysate was collected at 20-min intervals in tubes containing 5 μL of 5 mM ascorbic acid to prevent DA oxidation. After a 1-h settling period, five samples were collected to evaluate the baseline release of DA. Basal ACSF was then replaced first by ACSF fluid containing 10 μM cocaine and then 50 mM K^+, and four supplementary samples from each condition

were collected. Finally, the probes were perfused with ACSF containing 1 μM tetrodotoxin to assay the blockade of DA release following voltage-gated Na^{2+} channels inhibition. At the end of the experiment, mice were killed by decapitation and brains were quickly removed and put in 10% formalin, to verify the correct placement of the microdialysis probe. A total of 6–8 animals for each experimental group was analyzed. DA content in the dialysate samples was assessed by a researcher blind to the experimental conditions by using an ultra-HPLC (UHPLC, ALEXYS Neurotransmitter analyzer, Antec) equipped with a column NeuroSep (C18 110, 1.0 × 100 mm, 1.7 μm) and an electrochemical amperometric detector (DECADE II SCC). The mobile phase comprised 100 mM phosphoric acid, 100 mM citric acid, 0.1 mM EDTA, and acetonitrile (8% v/v), 3 mM.

Transmitted electron microscopy-based ultrastructural morphological analysis

For TEM imaging, samples from three animals per experimental group were processed according to Ferrarese and Lunardi,[40] with slight modifications. Briefly, animals were anesthetized and perfused as described above. Brain coronal sections (25 μm of thickness) were fixed in 2.5% glutaraldehyde in 0.3 M cacodylate buffer overnight at 4°C. Sections were then post-fixed in 1% osmium tetroxide (Electron Microscopy Sciences, Hatfield, PA, USA) for 1 h at 4°C, following dehydration and embedding in Epoxy resin (Sigma-Aldrich). Subsequently, 80- to 100-nm-thick ultrathin sections of the striatal areas of each sample were obtained using a diamond knife, collected on formvar coated grids, double stained with 1% uranyl acetate and 0.3% lead citrate, and observed with a Tecnai G2 (FEI) transmission electron microscope operating at 100 kV. Images were captured with a Veleta (Olympus Soft Imaging System) digital camera and analyzed with FIJI software. The morphometric analysis of pre-synaptic terminals was performed on a minimum of 60 synapses for each experimental group. The SVs were annotated manually in each pre-synaptic terminal. The vesicles density was calculated as number of vesicles/synapse area (nm^2). For each synapse, vesicles clustering was calculated as distance (nm) between vesicles centroid with the NND plugin and expressed as frequency distribution analyzed by multiple-peak Gaussian fit. Vesicle size was expressed as frequency distribution of the Feret diameter (nm) of vesicles in each synapse and analyzed by Gaussian fit. Finally, the vesicle distance from the active zone was expressed as frequency distribution of the distances (nm) between the centroid of each vesicle and the active zone, identified on the membrane of the pre-synaptic terminal in correspondence of the darker signal of the post-synaptic density. The striata of three animals for each experimental condition were analyzed. All measurements and counts were made on coded samples by an experimenter blind to the different experimental groups.

Statistical analysis

Statistical differences between groups were assessed as described in figure legends. Statistical significance was established at $P < 0.05$. The number (n) of animals used for each experimental group in the different experimental studies ranged between 3 and 10.

SUPPLEMENTAL INFORMATION

Supplemental information can be found online at https://doi.org/10.1016/j.ymthe.2022.01.021.

ACKNOWLEDGMENTS

We are grateful to Prof. Michel Goedert, MRC Laboratory of Molecular Biology, Cambridge, UK, for his support in the use of HS-68 luminescent-conjugated oligothiophene. We would also like to thank Dr. Francesco Boldrin for the remarkable work in sample processing and imaging at TEM at the DiBio Imaging Facility at the University of Padova (Italy).

This work was supported by The Michael J. Fox Foundation for Parkinson's Research, NY, USA (Target Advancement Program, grant ID #10742.01) to A.B.

AUTHOR CONTRIBUTIONS

A.B., G.F., and L.B. contributed to the study conception and design. Material preparation, data collection, and analysis were performed by G.F., F.L., A.M., V.B., R.F., T.K., H.S., E.P., and V.B. A.B., L.B., K.P.R.N., M.P., and M.G.S. supervised different aspects of the project. The first draft of the manuscript was written by G.F. and A.B., and all authors commented on previous versions of the manuscript. All authors read and approved the final manuscript.

DECLARATION OF INTERESTS

The authors have declared that no conflict of interest exists.

REFERENCES

1. Spillantini, M.G., Schmidt, M.L., Lee, V.M., Trojanowski, J.Q., Jakes, R., and Goedert, M. (1997). Alpha-synuclein in Lewy bodies. Nature *388*, 839–840. https://doi.org/10.1038/42166.

2. Engelender, S., and Isacson, O. (2017). The threshold theory for Parkinson's disease. Trends Neurosci. *40*, 4–14. https://doi.org/10.1016/j.tins.2016.10.008.

3. Lema Tome, C.M., Tyson, T., Rey, N.L., Grathwohl, S., Britschgi, M., and Brundin, P. (2013). Inflammation and alpha-synuclein's prion-like behavior in Parkinson's disease–is there a link? Mol. Neurobiol. *47*, 561–574. https://doi.org/10.1007/s12035-012-8267-8.

4. Longhena, F., Faustini, G., Spillantini, M.G., and Bellucci, A. (2019). Living in promiscuity: the multiple partners of alpha-synuclein at the synapse in physiology and pathology. Int. J. Mol. Sci. *20*, 141. https://doi.org/10.3390/ijms20010141.

5. Somayaji, M., Cataldi, S., Choi, S.J., Edwards, R.H., Mosharov, E.V., and Sulzer, D. (2020). A dual role for alpha-synuclein in facilitation and depression of dopamine release from substantia nigra neurons in vivo. Proc. Natl. Acad. Sci. U S A *117*, 32701–32710. https://doi.org/10.1073/pnas.2013652117.

6. Zaltieri, M., Grigoletto, J., Longhena, F., Navarria, L., Favero, G., Castrezzati, S., Colivicchi, M.A., Della Corte, L., Rezzani, R., Pizzi, M., et al. (2015). alpha-synuclein and synapsin III cooperatively regulate synaptic function in dopamine neurons. J. Cell Sci. *128*, 2231–2243. https://doi.org/10.1242/jcs.157867.

7. Bellucci, A., Mercuri, N.B., Venneri, A., Faustini, G., Longhena, F., Pizzi, M., Missale, C., and Spano, P. (2016). Review: Parkinson's disease: from synaptic loss to connectome dysfunction. Neuropathol. Appl. Neurobiol. *42*, 77–94. https://doi.org/10.1111/nan.12297.

8. Kile, B.M., Guillot, T.S., Venton, B.J., Wetsel, W.C., Augustine, G.J., and Wightman, R.M. (2010). Synapsins differentially control dopamine and serotonin release. J. Neurosci. *30*, 9762–9770. https://doi.org/10.1523/JNEUROSCI.2071-09.2010.

9. Longhena, F., Faustini, G., Varanita, T., Zaltieri, M., Porrini, V., Tessari, I., Poliani, P.L., Missale, C., Borroni, B., Padovani, A., et al. (2018). Synapsin III is a key

component of alpha-synuclein fibrils in Lewy bodies of PD brains. Brain Pathol. *28*, 875–888. https://doi.org/10.1111/bpa.12587.

10. Faustini, G., Longhena, F., Bruno, A., Bono, F., Grigoletto, J., La Via, L., Barbon, A., Casiraghi, A., Straniero, V., Valoti, E., et al. (2020). Alpha-synuclein/synapsin III pathological interplay boosts the motor response to methylphenidate. Neurobiol. Dis. *138*, 104789. https://doi.org/10.1016/j.nbd.2020.104789.

11. Faustini, G., Longhena, F., Varanita, T., Bubacco, L., Pizzi, M., Missale, C., Benfenati, F., Bjorklund, A., Spano, P., and Bellucci, A. (2018). Synapsin III deficiency hampers alpha-synuclein aggregation, striatal synaptic damage and nigral cell loss in an AAV-based mouse model of Parkinson's disease. Acta Neuropathol. *136*, 621–639. https://doi.org/10.1007/s00401-018-1892-1.

12. Reyes, A., Castillo, A., Castillo, J., and Cornejo, I. (2018). The effects of respiratory muscle training on peak cough flow in patients with Parkinson's disease: a randomized controlled study. Clin. Rehabil. *32*, 1317–1327. https://doi.org/10.1177/0269215518774832.

13. Moreau, C., Delval, A., Defebvre, L., Dujardin, K., Duhamel, A., Petyt, G., Vuillaume, I., Corvol, J.C., Brefel-Courbon, C., Ory-Magne, F., et al. (2012). Methylphenidate for gait hypokinesia and freezing in patients with Parkinson's disease undergoing subthalamic stimulation: a multicentre, parallel, randomised, placebo-controlled trial. Lancet Neurol. *11*, 589–596. https://doi.org/10.1016/S1474-4422(12)70106-0.

14. Casiraghi, A., Longhena, F., Straniero, V., Faustini, G., Newman, A.H., Bellucci, A., and Valoti, E. (2020). Design and synthesis of fluorescent methylphenidate Analogues for a FRET-based assay of synapsin III binding. ChemMedChem *15*, 1330–1337. https://doi.org/10.1002/cmdc.202000128.

15. Tofaris, G.K., Garcia Reitbock, P., Humby, T., Lambourne, S.L., O'Connell, M., Ghetti, B., Gossage, H., Emson, P.C., Wilkinson, L.S., Goedert, M., and Spillantini, M.G. (2006). Pathological changes in dopaminergic nerve cells of the substantia nigra and olfactory bulb in mice transgenic for truncated human alpha-synuclein(1-120): implications for Lewy body disorders. J. Neurosci. *26*, 3942–3950. https://doi.org/10.1523/JNEUROSCI.4965-05.2006.

16. Garcia-Reitbock, P., Anichtchik, O., Bellucci, A., Iovino, M., Ballini, C., Fineberg, E., Ghetti, B., Della Corte, L., Spano, P., Tofaris, G.K., et al. (2010). SNARE protein redistribution and synaptic failure in a transgenic mouse model of Parkinson's disease. Brain *133*, 2032–2044. https://doi.org/10.1093/brain/awq132.

17. Garcia-Reitboeck, P., Anichtchik, O., Dalley, J.W., Ninkina, N., Tofaris, G.K., Buchman, V.L., and Spillantini, M.G. (2013). Endogenous alpha-synuclein influences the number of dopaminergic neurons in mouse substantia nigra. Exp. Neurol. *248*, 541–545. https://doi.org/10.1016/j.expneurol.2013.07.015.

18. Longhena, F., Faustini, G., Brembati, V., Pizzi, M., Benfenati, F., and Bellucci, A. (2021). An updated reappraisal of synapsins: structure, function and role in neurological and psychiatric disorders. Neurosci. Biobehav. Rev. *130*, 33–60. https://doi.org/10.1016/j.neubiorev.2021.08.011.

19. Baldelli, P., Fassio, A., Valtorta, F., and Benfenati, F. (2007). Lack of synapsin I reduces the readily releasable pool of synaptic vesicles at central inhibitory synapses. J. Neurosci. *27*, 13520–13531. https://doi.org/10.1523/JNEUROSCI.3151-07.2007.

20. Gry, M., Rimini, R., Stromberg, S., Asplund, A., Ponten, F., Uhlen, M., and Nilsson, P. (2009). Correlations between RNA and protein expression profiles in 23 human cell lines. BMC Genomics *10*, 365. https://doi.org/10.1186/1471-2164-10-365.

21. Perl, K., Ushakov, K., Pozniak, Y., Yizhar-Barnea, O., Bhonker, Y., Shivatzki, S., Geiger, T., Avraham, K.B., and Shamir, R. (2017). Reduced changes in protein compared to mRNA levels across non-proliferating tissues. BMC Genomics *18*, 305. https://doi.org/10.1186/s12864-017-3683-9.

22. Klingstedt, T., Ghetti, B., Holton, J.L., Ling, H., Nilsson, K.P.R., and Goedert, M. (2019). Luminescent conjugated oligothiophenes distinguish between alpha-synuclein assemblies of Parkinson's disease and multiple system atrophy. Acta Neuropathol. Commun. *7*, 193. https://doi.org/10.1186/s40478-019-0840-1.

23. Shahnawaz, M., Mukherjee, A., Pritzkow, S., Mendez, N., Rabadia, P., Liu, X., Hu, B., Schmeichel, A., Singer, W., Wu, G., et al. (2020). Discriminating alpha-synuclein strains in Parkinson's disease and multiple system atrophy. Nature *578*, 273–277. https://doi.org/10.1038/s41586-020-1984-7.

24. Klingstedt, T., Shirani, H., Aslund, K.O., Cairns, N.J., Sigurdson, C.J., Goedert, M., and Nilsson, K.P. (2013). The structural basis for optimal performance of oligothiophene-based fluorescent amyloid ligands: conformational flexibility is essential for spectral assignment of a diversity of protein aggregates. Chemistry *19*, 10179–10192. https://doi.org/10.1002/chem.201301463.

25. Kovacs, G.G., Wagner, U., Dumont, B., Pikkarainen, M., Osman, A.A., Streichenberger, N., Leisser, I., Verchere, J., Baron, T., Alafuzoff, I., et al. (2012). An antibody with high reactivity for disease-associated alpha-synuclein reveals extensive brain pathology. Acta Neuropathol. *124*, 37–50. https://doi.org/10.1007/s00401-012-0964-x.

26. Delenclos, M., Faroqi, A.H., Yue, M., Kurti, A., Castanedes-Casey, M., Rousseau, L., Phillips, V., Dickson, D.W., Fryer, J.D., and McLean, P.J. (2017). Neonatal AAV delivery of alpha-synuclein induces pathology in the adult mouse brain. Acta Neuropathol. Commun. *5*, 51. https://doi.org/10.1186/s40478-017-0455-3.

27. Tang, Y., Scott, D., Das, U., Gitler, D., Ganguly, A., and Roy, S. (2013). Fast vesicle transport is required for the slow axonal transport of synapsin. J. Neurosci. *33*, 15362–15375. https://doi.org/10.1523/JNEUROSCI.1148-13.2013.

28. Schulz-Schaeffer, W.J. (2010). The synaptic pathology of alpha-synuclein aggregation in dementia with Lewy bodies, Parkinson's disease and Parkinson's disease dementia. Acta Neuropathol. *120*, 131–143. https://doi.org/10.1007/s00401-010-0711-0.

29. Wang, L., Das, U., Scott, D.A., Tang, Y., McLean, P.J., and Roy, S. (2014). alpha-synuclein multimers cluster synaptic vesicles and attenuate recycling. Curr. Biol. *24*, 2319–2326. https://doi.org/10.1016/j.cub.2014.08.027.

30. Bellucci, A., Navarria, L., Falarti, E., Zaltieri, M., Bono, F., Collo, G., Spillantini, M.G., Missale, C., and Spano, P. (2011). Redistribution of DAT/alpha-synuclein complexes visualized by "in situ" proximity ligation assay in transgenic mice modelling early Parkinson's disease. PLoS One *6*, e27959. https://doi.org/10.1371/journal.pone.0027959.

31. Chu, Y., Muller, S., Tavares, A., Barret, O., Alagille, D., Seibyl, J., Tamagnan, G., Marek, K., Luk, K.C., Trojanowski, J.Q., et al. (2019). Intrastriatal alpha-synuclein fibrils in monkeys: spreading, imaging and neuropathological changes. Brain *142*, 3565–3579. https://doi.org/10.1093/brain/awz296.

32. Longhena, F., Faustini, G., Missale, C., Pizzi, M., and Bellucci, A. (2018). Dopamine transporter/alpha-synuclein complexes are altered in the post mortem caudate putamen of Parkinson's disease: an in situ proximity ligation assay study. Int. J. Mol. Sci. *19*, 1611. https://doi.org/10.3390/ijms19061611.

33. Venton, B.J., Seipel, A.T., Phillips, P.E., Wetsel, W.C., Gitler, D., Greengard, P., Augustine, G.J., and Wightman, R.M. (2006). Cocaine increases dopamine release by mobilization of a synapsin-dependent reserve pool. J. Neurosci. *26*, 3206–3209. https://doi.org/10.1523/JNEUROSCI.4901-04.2006.

34. Scott, D.A., Tabarean, I., Tang, Y., Cartier, A., Masliah, E., and Roy, S. (2010). A pathologic cascade leading to synaptic dysfunction in alpha-synuclein-induced neurodegeneration. J. Neurosci. *30*, 8083–8095. https://doi.org/10.1523/JNEUROSCI.1091-10.2010.

35. Westphal, C.H., and Chandra, S.S. (2013). Monomeric synucleins generate membrane curvature. J. Biol. Chem. *288*, 1829–1840. https://doi.org/10.1074/jbc.M112.418871.

36. Diao, J., Burre, J., Vivona, S., Cipriano, D.J., Sharma, M., Kyoung, M., Sudhof, T.C., and Brunger, A.T. (2013). Native alpha-synuclein induces clustering of synaptic-vesicle mimics via binding to phospholipids and synaptobrevin-2/VAMP2. eLife *2*, e00592. https://doi.org/10.7554/eLife.00592.

37. Calo, L., Hidari, E., Wegrzynowicz, M., Dalley, J.W., Schneider, B.L., Podgajna, M., et al. (2021). CSPalpha reduces aggregates and rescues striatal dopamine release in alpha-synuclein transgenic mice. Brain. *144*, 1661–1669. https://doi.org/10.1093/brain/awab076.

38. Paxinos, G. (2012). Paxinos and Franklin's the Mouse Brain in Stereotaxic Coordinates, fourth edition (Elsevier Academic Press).

39. Fleming, S.M., Ekhator, O.R., and Ghisays, V. (2013). Assessment of sensorimotor function in mouse models of Parkinson's disease. J. Vis. Exp. e50303. https://doi.org/10.3791/50303.

40. Ferrarese, B., and Lunardi, N. (2019). Preparation of newborn rat brain tissue for ultrastructural morphometric analysis of synaptic vesicle distribution at nerve terminals. J. Vis. Exp. *148*, e59694. https://doi.org/10.3791/59694.